Pergamon

Geochimica et Cosmochimica Acta, Vol. 65, No. 8, pp. 1187–1210, 2001

0016-7037/01 $20.00 + .00

PII S0016-7037(00)00617-7

The transport of U- and Th-series nuclides in a sandy unconfined aquifer

A. TRICCA,[1] G. J. WASSERBURG,[1,*] D. PORCELLI,[1,†] and M. BASKARAN[2]

[1]The Lunatic Asylum of the Charles Arms Laboratory, Division of Geological and Planetary Sciences, California Institute of Technology, Pasadena, CA 91125 USA

[2]Department of Geology, Wayne State University, Detroit, MI 48202, USA

(*Received March* 24, 2000; *accepted in revised form November* 29, 2000)

Abstract—A comprehensive evaluation of the transport of U, Th, Ra, and Rn nuclides of the ^{238}U- and ^{232}Th-decay series in an unconfined sandy aquifer (Long Island, NY) was conducted. Groundwater data are compared with results of a theoretical transport model of weathering of aquifer grains and interaction with surface coatings to establish relationships between the concentrations of the radionuclide activities in the water and flow line distance. The data provide estimates for geochemical parameters including weathering rates and chemical reactivities in both the vadose zone and the aquifer. A theoretical treatment of the transport is presented that considers the reaction between the water and a reactive surface layer. It is found that a model with chemical exchange between the surface layer and the water for all species is not valid, and that the effects of saturation and "irreversible" precipitation of Th is required.

The water table shows a relatively wide range in U activities, the only element in the U-Th series for which vadose zone input is significant in the aquifer. High weathering of U and recoil inputs of ^{234}U to the water occur in the upper 3 m of the vadose zone, while lower weathering and removal of U from the water occur below. The deeper aquifer has variable ^{238}U activities that can be accounted for by input from the vadose zone and is not a result of non-conservative behavior. The isotopic composition of U is shown to be directly related to the recoil rate relative to the weathering rate. The wide range of ^{238}U in the aquifer waters is a reflection of diverse vadose zone inputs, showing that dispersive mixing is not a dominant effect. The higher values of δ^{234}U in the aquifer reflect the recoil/weathering input ratios from within the aquifer where the weathering rate is lower than the vadose zone. Both high U activities and high δ^{234}U values cannot be obtained in the vadose zone or within reasonable flow distances in the aquifer. Radium isotopes are found to be in exchange equilibrium with the surface layer. ^{224}Ra, ^{228}Ra, and ^{226}Ra have comparable activities throughout the aquifer. In the vadose zone, the dominant input of Ra to groundwater is weathering and recoil. As found elsewhere, the ^{222}Rn in the water is a large fraction ($\sim$5%) of the Rn produced in the aquifer rock. This cannot be due to Ra precipitation onto surface coatings in the aquifer as supported by present weathering with Th in exchange equilibrium with the surface layer. It is found that Th is saturated in the waters under oxidizing conditions so that the weathering input is irreversibly precipitating onto surfaces. However, it is shown that under somewhat reducing conditions, Th activities are much higher and the Th/U ratio in the solution is approximately that of the rock. We propose that under oxidizing conditions the source of Rn is a surface coating enriched in ^{232}Th and ^{230}Th. This Th was precipitated in an earlier phase during rapid dissolution of readily weathered phases that contain $\sim$10% of the U-Th inventory of the rock, with the associated U carried away in solution. Therefore, the previously precipitated ^{230}Th and ^{232}Th produce daughter nuclides in the surface coating which are the dominant contributors of Ra and Rn to the ground water. In particular, Rn is provided by very efficient losses (by diffusion or recoil) from the surface coating. This then does not require recent, large recoil losses from the parent rock or the presence of nanopores in the rock. The first data of both long-lived ^{232}Th and short-lived ^{234}Th and ^{228}Th in ground water is reported. The Th isotope activities indicate that desorption kinetics are slow and provide the first estimate, based on field data, of the Th desorption rate from an aquifer surface. The mean residence time of Th in the surface coating is $\sim$3000 y while in the water it is $\sim$1 h. Ra is in partition equilibrium with the aquifer surface layer. However, the strong fixation of Th on surface coatings is very susceptible to changes in oxidation state as is shown by a comparison of two adjacent aquifers. This makes it difficult to define with certainty the retentive characteristics in natural systems. In general, it is shown that the distributions of naturally occurring nuclides can be used to calculate values for transport parameters that are applicable to the transport of anthropogenic nuclides.

1. INTRODUCTION

Naturally occurring radionuclides provide analogues for pollutant nuclides. The behavior of U, Th, Ra and Rn isotopes can be studied through their relationships in the ^{238}U and ^{232}Th decay series where the half lives are given in parentheses:

*Author to whom correspondence should be addressed (isotopes@gps.caltech.edu).

† *Present address:* Institute for Isotope Geology and Mineral Resources, ETH 8092 Zurich, Switzerland

$$^{238}\mathrm{U}(4.5\mathrm{Ga}) \xrightarrow{\alpha} {}^{234}\mathrm{Th}(24\mathrm{d}) \xrightarrow{\beta} {}^{234}\mathrm{U}(0.25\mathrm{Ma}) \xrightarrow{\alpha} {}^{230}\mathrm{Th}(75\mathrm{ka}) \xrightarrow{\alpha} {}^{226}\mathrm{Ra}(1.6\mathrm{ka}) \xrightarrow{\alpha} {}^{222}\mathrm{Rn}(3.8\mathrm{d})$$

$$^{232}\mathrm{Th}(14\mathrm{Ga}) \xrightarrow{\alpha} {}^{228}\mathrm{Ra}(5.8\mathrm{a}) \xrightarrow{\beta} {}^{228}\mathrm{Th}(1.9\mathrm{a}) \xrightarrow{\alpha} {}^{224}\mathrm{Ra}(3.6\mathrm{d})$$

These two decay chains permit comparison of the behavior of two isotopes of the same element which are assumed to have the same chemical properties but very different lifetimes (two isotopes of U, three isotopes of Th, two isotopes of Ra). Although the U-Th series nuclides are expected to be in secular equilibrium in unaltered aquifer host rocks, examples of pronounced disequilibria are found in groundwater. This clearly shows that in open systems such as aquifers, water-rock interactions induce significant elemental and isotopic fractionations (see e.g., Osmond and Cowart, 1992). While the thermodynamic properties of these elements in aqueous solutions under laboratory conditions are well known (see Langmuir, 1997), it is difficult to predict behavior in more complex natural systems. Several studies have considered the aquifer transport of U-Th series nuclides (see Ku et al., 1992; Cowart and Burnett, 1994). Andrews and Kay (1982) and Andrews et al. (1989) calculated the time-scales for nuclide supply and removal. Krishnaswami et al. (1982) calculated supply rates, sorption rate constants, and residence times of short-lived nuclides by deducing recoil inputs of U-Th series nuclides from ^{222}Rn activities, but did not consider dissolution, precipitation, and advective transport. Davidson and Dickson (1986) included dispersive flow for U and Ra, but not dissolution and precipitation.

This study uses data from an unconfined sandy aquifer to understand the transport of naturally occurring U, Th, Ra, and Rn nuclides. The approach here differs from earlier works in using a unified transport model by considering:

1. more complete sequences of U, Th, Ra and Rn nuclides within the ^{238}U- and ^{232}Th-decay series;
2. the vadose zone input into the aquifer through analysis of waters from water table wells;
3. the interactions with the aquifer solid through sampling waters of different "ages";
4. the distribution of radionuclides between different filtration size fractions;
5. the relationship of the observed activities to a water flow model (Tricca et al., 2000) that includes vadose zone input, weathering and recoil within the aquifer and reaction with a surface layer.

A model is used to discuss the data that includes weathering, α-recoil, and a reactive surface coating on the aquifer mineral grains that plays a significant role in storage of Th and Ra radionuclides. If one assumes the sites are in exchange equilibrium with the water, it will be shown that this storage is inadequate to provide sufficient sources of ^{222}Rn. From experimental data, Th is close to the saturation limit with thorianite, which is not compatible with an exchange equilibrium model. A modified model is proposed where ^{230}Th and ^{232}Th are quasi irreversibly removed from the water and deposited on surface coating. This Th coating from an earlier stage of weathering can readily provide a surface layer sufficient to support ^{222}Rn.

The basic chemical interactions (both equilibrium and non-equilibrium) depend on the concentrations ($^{i}c_j$) of each species i in the different phases (j-water, rock, surface coating). However, as the U and Th decay series connect the production of nuclides along the chain by radioactive decay, the activity ($\lambda_i\ ^{i}c_j$) of each species is a governing parameter. We will therefore couch our representation of the transport problem in terms of activities and on occasion refer to the concentrations.

The approach used in this study was to choose a simple aquifer with generally known flow patterns and to follow the abundances of the U-Th series nuclides from the vadose zone input along flow lines. The intent was to determine the evolution of these nuclides along the flow path considering the vadose zone input and subsequent effects of water-rock interaction along the flow paths. This study uses the available hydrologic information available at the site. It does not depend upon the residence times as may be estimated from other tracers but upon the flow rates. The time and distance scales inferred from this study thus result from the rock-water interactions themselves using a typical flow velocity obtained by the hydrologic data. For a more extensive discussion of the theoretical model, the reader is referred to Tricca et al. (2000).

2. SAMPLING AND ANALYTICAL PROCEDURES

This study focuses on the unconfined Upper Glacial Aquifer in Long Island, NY (Figs. 1 and 2) within and around the DOE Brookhaven National Laboratory (BNL). The hydrogeology of the area has been described by de Laguna (1963), de Laguna (1966) and Warren et al. (1968). The aquifer consists of 30 to 70 m of unconsolidated Pleistocene sandy deposits overlain by an unsaturated zone (3–30 m). The aquifer and unsaturated zone consist of quartz, feldspars and traces of micaceous minerals, as well as U/Th bearing zircon and apatite (Faust, 1963; de Laguna, 1963). No carbonate or evaporite minerals were reported. Ground water flows at 1×10^{-4}–2×10^{-4} cm sec^{-1}; the upper value will be used for discussion here. There is an east-west groundwater divide north of the site, and flow across the study area is southward. Available piezometric data provide horizontal flow directions (see Fig. 2 and Geraghty and Miller, 1996), but not vertical flow rates, so unambiguously following the descent of flow lines is not possible. Yet, the ages of waters sampled by deep wells are likely to increase with greater distance from the groundwater divide (see Fig. 2). In this study, well lines have been selected to be along possible flow lines, although incorporation of waters that have evolved along different paths is also considered. The underlying Magothy aquifer is locally separated from the Upper Glacial aquifer by the confining Gardiner's Clay (0–10 m). These Magothy waters are under more reducing conditions and give key complementary data to that found in the Upper Glacial unit.

Ground waters were obtained to determine the vadose zone contribution to the aquifer and effect on the nuclide behavior along flow lines (Fig. 2 and Table 1). In October, 1997, samples were taken along two well lines (W and E) in the Upper Glacial Aquifer. Data for past Ethylene Dibromide contamination (BNL, pers. comm.) indicated that waters from wells E1(S)$_{wt}$ and E2(I) were on the same flowline. A sample was collected in the Magothy (M1) to characterize that aquifer. Note that water from the Magothy was yellow indicating the presence of organic carbon or Fe. No H_2S was detected in the Magothy waters. Other water table samples (W1(S)$_{wt}$, S1$_{wt}$, S2$_{wt}$, S3$_{wt}$) were collected in March, 1999 to study nuclide behavior in the vadose zone.

Ground water was drawn using a submersible pump run at 0.5 to 20

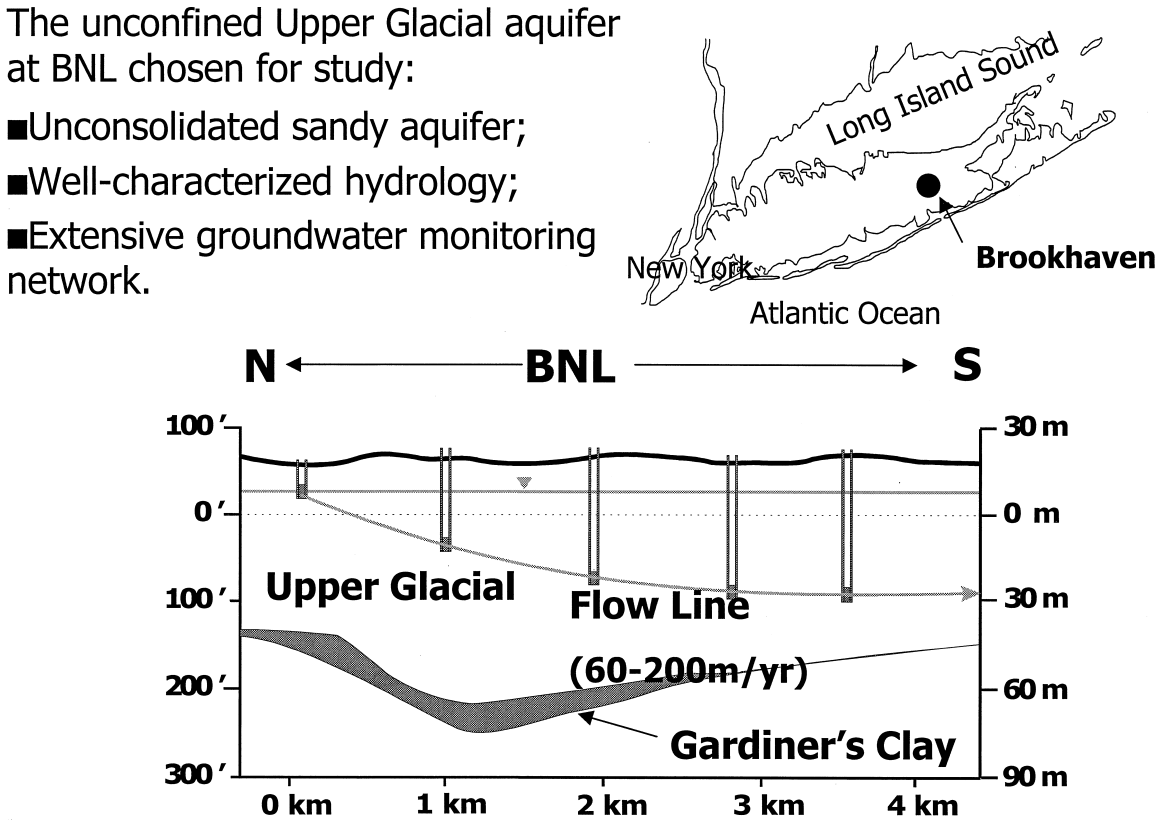

Fig. 1. Schematic diagram showing the location and general layout of the aquifer under investigation. Water table samples are from the base of the vadose zone. Aquifer samples from wells presumed to be along a flow line.

L/min. Temperature, pH, and dissolved O_2 concentrations were measured on site along with Rn. Oxygen was measured by O_2 diffusion with a YSI55 oxygen probe. During this measurement, the authors avoided exchange between the sample and the atmosphere. Major anions and cations, Fe, and Mn were measured by SGAB Analyses (Luleå, Sweden). For analysis of ^{238}U, ^{234}U, and ^{232}Th, separate water samples were collected either unfiltered or filtered on-line through 0.45 μm cellulose filters. A fraction of the filtered samples were further separated into colloids and 'dissolved' fractions using ultra-filtration systems with a nominal cut-off size of 10 k Daltons. Samples were ultra-filtered with Amicon® polyethersulfone hollow fiber cartridges (see e.g., Porcelli et al., 1997). All filtrations were done, and all samples were acidified, in the field. The filtration system was rinsed between each sample with 1N ultra-pure HCl to collect material remaining in the system. This rinse was kept for analysis. A second HCl rinse was circulated followed by ultrapure water. The ^{238}U, ^{234}U, and ^{232}Th of each fraction was concentrated and measured by mass spectrometry (Chen et al., 1986). For analysis of short-lived Ra and Th isotopes, 100 L samples were passed on-line through 0.45 μm prefilters and through Mn-oxide coated acrylic filters. The Mn-oxide filters were ashed and measured by α and γ counting at Texas A&M, Galveston (Baskaran et al., 1993). Absolute ^{226}Ra activities were determined from 20 L of 0.45 μm-filtered water, passed through Mn-oxide impregnated fibers that have high Ra adsorption efficiency (Reid et al., 1979).

Total recoveries for the ultra-filtration procedures were evaluated by comparing concentrations in 0.45 μm-filtered waters with the sum total recovery in $<$10 k D ultra-filtered water, $>$10 kD colloids, and HCl rinse. The U recovery for the Amicon ultra-filtration system for sample #W3(D) is only 75%. In addition, a significant amount of U appeared in the acid rinse that was retained during ultra-filtration. The $\delta^{234}U$ value (see Table 2 for definition) of the acid rinse shows that the U lost by adsorption belongs to the $<$10 kD fraction (Table 2). Therefore, the U concentration measured in the filtrate is a minimum value for "dissolved" U.

3. RESULTS

General chemical compositions of the samples are shown in Table 1. The total dissolved solids (TDs) are given in the standard units which include Si($\sim$10 mg/L) and K ($<$1 mg/L). The dominant ions are generally Na^+ and either HCO_3^- or Cl^-, with no systematic relationship. The waters are slightly acidic. Major element data for ultra-filtered waters were indistinguishable from those of corresponding 0.45 μm filtered samples and are not shown. The water table samples are oxidizing, with dissolved oxygen concentrations of 0.25 and 0.47 mM. These samples have the lowest pH values of the Upper Glacial Aquifer of 4.78 to 5.74 (compared to 5.74–6.09 for deeper wells), and also generally have the lowest TDS. Dissolved organic carbon concentrations are between 0.96 to 6.6 mg/L, and are typical for groundwater (see Stumm and Morgan, 1996). Only 0.42 to 0.95 mg/L DOC is associated with $>$ 10 kD colloids. The Total Dissolved Solid (TDS) concentrations are $<$100 mg/L (except W3(D)). The lack of correlation between TDS and distance from the recharge area or depth requires that the waters sampled on a single well-line have undergone substantially different evolutionary histories due to either changing interaction with the vadose zone, or mixing in the well of waters of different ages, or sampling from different flow lines with different aquifer input conditions. These issues will be evaluated further below. The elements (Ca, Mg, Na, HCO_3, Cl, $SO_4^=$ are in millimoles per liter (mM). Fe and Mn are given in micromoles per liter (μM). The Fe concentrations in the Upper

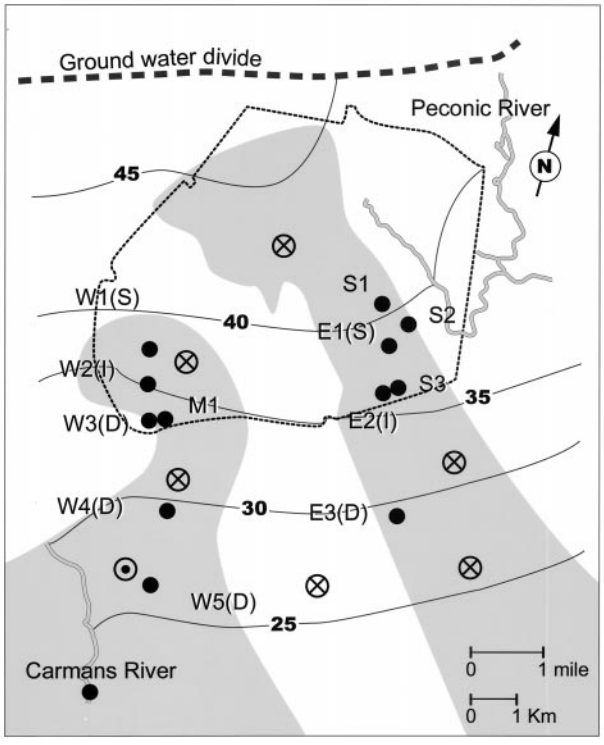

Fig. 2. The location of the wells sampled (●). Samples W and E were taken from the unconfined Upper Glacial Aquifer at either shallow (S), intermediate (I), or deep (D) levels below the water table. Sample M is from the confined Magothy Aquifer. The solid lines show the piezometric levels of the Upper Glacial aquifer. The gray area represents the surface of the Gardiner's Clay Unit discontinuously separating the Upper Glacial and Magothy aquifers. Downward (⊗) or upward (⊙) vertical flow across the Upper Glacial Aquifer/Magothy boundary is shown. Note the east-west trending groundwater divide located ~0.5 km north of the site.

Glacial are <0.2 μM (Table 1) which is in the lower range for ground waters (Hem, 1992). These concentrations are 10^3 larger than the solubility limit of Fe(III), and are too oxidized to form Fe(II); therefore Fe must be associated with colloids. The Mn concentrations are much lower than the solubility limit in the deeper wells (<0.02–0.16 μM), with the exception of E3(D), which has a concentration of 7.5 μM Mn close to the solubility limit that is common in ground waters (Hem, 1992). Therefore Mn is likely to be in the soluble Mn(II) form. For wells $E1(S)_{wt}$ to E2(I), located on the same flow line, the concentration of Cl, a conservative element, is doubled (see Table 1); this cannot be obtained by reasonable weathering rates of the aquifer solid. There is no halite or saline layer in the soil. Therefore, these Cl variations must reflect temporal changes of a surface input induced by anthropogenic inputs such as road salting.

The Magothy waters are chemically distinctive from those of the Upper Glacial Aquifer (Table 1), with lower dissolved oxygen (although no presence of H_2S was observed), higher pH (6.77) and very high Fe and Mn concentrations. The Fe concentration (214 μM) in the filtered water is $\sim 10^6$ times the solubility limit of Fe(III) (e.g., Fox, 1988, Stumm and Morgan, 1996). The dominant fraction of Fe (70%, see data, Table 1) did not pass through the 10 kD filter and so is likely to be colloidal Fe. The remaining 30%, 54 μM Fe/L, is still above the solubility limit and is plausibly contained in smaller colloidal particles). It is not due to dissolved organic carbon as the concentrations are the same level as in the overlying aquifer. The Mn concentration (25 μM) is substantially above the value of 2 μM commonly found in oxidizing ground waters elsewhere and is above the solubility limit of Mn(II) (Hem, 1992). Note that all the Mn is in the <10 kD fraction, (Table 1), and must be in colloids of size <10 kD or else the solubility is significantly enhanced. The high Mn concentration (e.g., the Mn/Mg ratio is ~10 times that of upper crustal rocks, (Taylor and McLennan, 1985)) could be due to release of Mn oxyhydroxides previously deposited under different redox conditions (Section 5 on Thorium).

Sr was measured in samples from the Upper Glacial and Magothy (Table 2 and Fig. 3). Water table samples have higher $^{87}Sr/^{86}Sr$ ratios (0.71191–0.71357) than the deeper samples (0.71144–0.71163) indicating that Sr provided by mineral weathering in the aquifer is less radiogenic than that provided at the water table. The Sr isotopic ratios in the deep wells are indistinguishable from in the Magothy, where $^{87}Sr/^{86}Sr = 0.71144$, suggesting that the deep ground water flows through host rocks of composition similar to that of the Magothy. Sr concentrations range from 12 to 53 μg/kg in no simple pattern.

For the U-Th series nuclides, we will present the data in terms of specific activity of nuclide i in a given phase (j) (^iA_j) (disintegrations per minute per kg). The relative isotopic abundance of ^{234}U in waters (w) will be given by $\delta^{234}U \equiv (^{234}U A_w / ^{238}U A_w - 1) \times 10^3$ (see Table 2).

The ^{238}U activities in the aquifer (<0.45 μm) vary within 2×10^{-3} to 18×10^{-3} dpm/kg (3–24 ng/kg). This is in the lower part of the extreme range reported for ground waters of 2×10^{-3} to 10^3 μg/kg (Osmond and Ivanovich, 1992). They have $\delta^{234}U = 30$ to 1400‰ and so are all enriched in ^{234}U. Water table U activities vary between 1.1×10^{-3} to 1.9×10^{-2} dpm/kg. This range covers all activities measured in the aquifer. Therefore, U input from the vadose zone to the aquifer can represent an important portion of the U within the

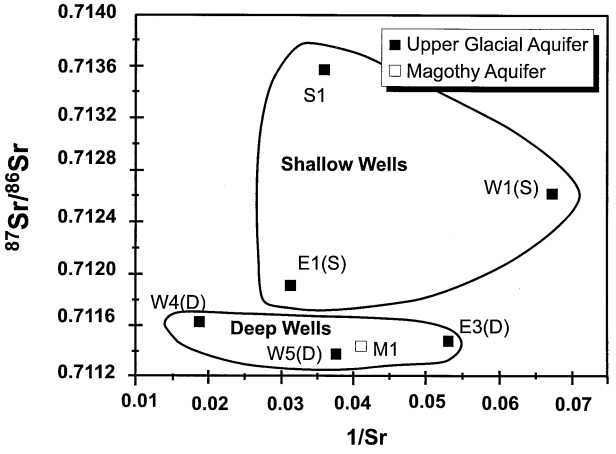

Fig. 3. Sr data of filtered samples from the Upper Glacial and Magothy Aquifers. Samples from deep wells within both aquifers have similar $^{87}Sr/^{86}Sr$ ratios, and are distinct from those of water table samples. Note that for a two-component mixing model, the relationship is of the form $(^{87}Sr/^{86}Sr) = A + B/Sr$.

Table 1. General characteristics of groundwater samples.[a]

Well #	BNL #	Water level[b] m	depth[c] m	TDS[d] mg/l	pH	O_2[e] mM	DOC (mg/l) <0.45 μm	DOC (mg/l) Colloids	DOC (mg/l) <10 kD	Ca_2 mM	Mg mM	Na mM	HCO_3 mM	Cl mM	SO_4 mM	Fe[f] μM	Mn[d] μM
West line																	
$W1(S)_{wt}a$[g]	93-04	15	0–5	33	5.42	0.49	1.92	—	1.02	0.06	0.05	0.21	0.07	0.23	0.08	0.05	0.036
$W1(S)_{wt}b$[h]	93-04	15	0	29	5.40	—	—	—	—	0.05	0.05	0.19	<0.16	0.16	0.10	0.05	0.13
W2(I)	118-02	15	27	76	5.62	0.31	3.29	—	—	0.15	0.11	0.58	0.16	0.68	0.10	0.12	0.05
W3(D)	130-03	15	40	119	6.09	0.13	1.34	0.42	1.03	0.27	0.20	0.70	0.44	0.79	0.16	<0.007	<0.02
W4(D)	000-98	24	43	56	5.74	0.31	1.95	—	—	0.10	0.08	0.44	0.14	0.59	0.04	0.09	0.15
W5(D)	800-40	19	43	62	5.95	0.16	6.61	0.86	5.29	0.12	0.09	0.30	0.43	0.20	0.06	0.05	0.16
East line																	
$E1(S)_{wt}$	79-17	4	0–5	91	5.74	0.25	1.56	0.46	0.88	0.32	0.22	0.12	0.33	0.17	0.19	0.014	0.13
E2 (I)	100-14	4	30	55	6.03	0.19	1.55	0.95	0.59	0.12	0.10	0.29	0.21	0.37	0.06	<0.007	<0.02
E3(D)	800-25	6	47	42	6.5	0.22	0.96	—	0.61	0.08	0.05	0.23	0.25	0.20	0.05	0.02	7.5
Magothy																	
M1	130-04	16	250	66	6.77	0.06	5.14	0.70	2.52	0.17	0.08	0.25	0.52	0.20	0.03	214	25
$M1_{<10kD\ fraction}$										0.16	0.09	0.25	—	—	—	54	24.5
Water table																	
$S1_{wt}$	58-01	3	0	27	4.82	—	—	—	—	0.03	0.04	0.19	<0.16	0.14	0.09	<0.9	0.35
$S2_{wt}$	100-10	3	0	28	4.95	—	—	—	—	0.04	0.10	0.11	<0.16	0.07	0.15	<0.9	0.13
$S3_{wt}$	70-01	7	0	24	4.78	—	—	—	—	<0.02	0.05	0.20	<0.16	0.16	0.08	<0.9	0.65

[a] The units: m(meters); mg/l = milligrams/liter; mM = millimoles/liter; μM = micromoles/liter.
[b] Water table level given in meters below surface level.
[c] Depth of water samples, given in meters below water table.
[d] Total Dissolved Load (values include the concentrations of K and Si, not given in the table).
[e] O_2 saturation with the atmosphere $\approx$0.4 mM.
[f] Data within 5% error measured by Svensk Grundämnesanalys AB, Luleå Tekn. Universitet, 971 87 Luleå, Sweden.
[g] Sample collected Fall 97.
[h] Sample collected Spring 99.

Table 2. U and Th activities in the water samples.

Well	^{238}U (10^{-3} dpm/kg)			$\delta^{234}U$[a]			^{234}U Excess (10^{-3} dpm/kg)	^{232}Th (10^{-5} dpm/kg)		Sr (ppb)	$^{87}Sr/^{86}Sr$
	Unfiltered	<0.45 μm	<10 kD	Unfiltered	<0.45 μm	<10 kD	<0.45 μm	Unfiltered	<0.45 μm	<0.45 μm	<0.45 μm
West line											
$W1(S)_{wt}a$[b]	—	2.839 ± 0.006	0.341 ± 0.002	—	46 ± 12	—	0.13	—	2.38 ± 0.01	14.87	0.71262 ± 4
$W1(S)_{wt}b$[c]	—	3.47 ± 0.01	—	—	—	—	—		11.6 ± 0.1	19	—
W2(I)	—	3.817 ± 0.007	2.047 ± 0.007	—	615 ± 18	172 ± 16	2.35	—	4.03 ± 0.02	40	—
W3(D)	10.71 ± 0.04	12.15 ± 0.05	2.570 ± 0.007	166 ± 22	130 ± 11	128 ± 11	1.58	22.6 ± 0.2	1.09 ± 0.02	27	—
W4(D)	—	6.551 ± 0.003	0.822 ± 0.003	—	1394 ± 23	917 ± 24	9.13	—	1.42 ± 0.007	53.49	0.71163 ± 5
W4(D)[d]	—	6.535 ± 0.002	—	—	1390 ± 19	—	9.08	—	—	—	—
W5	—	2.87 ± 0.01	0.2730 ± 0.0007	—	673 ± 33	—	1.93	—	0.700 ± 0.005	24.39	0.71138 ± 5
East line											
$E1(S)_{wt}$	—	5.36 ± 0.03	—	—	31 ± 17	—	0.17	—	1.244 ± 0.007	31.9	0.71191 ± 6
E2(I)	—	10.04 ± 0.03	—	—	40 ± 9	—	0.40	—	0.342 ± 0.004	19	—
E3(D)	—	2.122 ± 0.007	0.1326 ± 0.0003	—	332 ± 21	388 ± 131	0.70	—	0.464 ± 0.002	18.9	0.71148 ± 7
Magothy											
M1	35.1 ± 0.5	18.9 ± 0.7	7.53 ± 0.03		197 ± 11	112 ± 15	3.72	6571 ± 20	2148 ± 20	26.61	0.71144 ± 5
Water table											
$S1_{wt}$	—	18.07 ± 0.04	—		44 ± 13	—	0.80	—	—	27.8	0.71357 ± 7
$S2_{wt}$	—	1.083 ± 0.007	—		698 ± 29	—	0.76	—	—	12	—
$S3_{wt}$	—	3.12 ± 0.007	—	—	39 ± 11	—	0.12	—	—	18	—

[a] $\delta^{234}U$ is the isotopic shift in permil deviation from secular equilibrium $\delta^{234}U_w=(^{234U}A_w/^{238U}A_w-1)\times 10^3$ and $^{234U}A_w$ and $^{238U}A_w$ are the activities of ^{234}U and ^{238}U in the water.

[b] Sample collected in Fall 97.

[c] Sample collected in Spring 99.

[d] Duplicate.

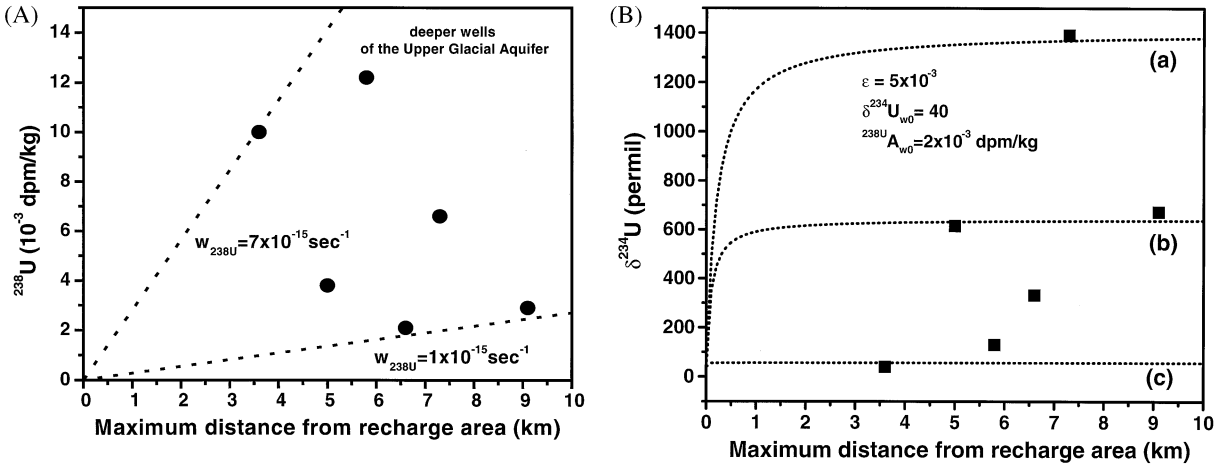

Fig. 4. (A) ^{238}U activities from deep wells in the Upper Glacial Aquifer. The distance of each well from the groundwater divide to the north (see Fig. 2) is plotted; there is no correlation of activity with this distance. The slopes of the dashed lines define the weathering rates yielding the sample U activities assuming no U input from the vadose zone. (B) $\delta^{234}U_w$ from deep wells in the Upper Glacial Aquifer. The dashed lines show the model evolution of $\delta^{234}U_w$ along flow lines for (a) $w_{238_U} = 3 \times 10^{-16}$ sec^{-1}, (b) $w_{238_U} = 7 \times 10^{-16}$ sec^{-1}, and (c) $w_{238_U} = 8 \times 10^{-15}$ sec^{-1}.

aquifer fluid. The U activity in well W1(S)$_{wt}$ varies by ~18% between two sampling dates. U activities at the water table (symbol "wt") are not correlated with the thickness of the overlying vadose zone; wells S1$_{wt}$ and S2$_{wt}$, where the unsaturated zone is ~3 m thick, have the highest and lowest ^{238}U activities, respectively (Table 2). The water table samples usually show moderate U disequilibria ($\delta^{234}U = 31-46‰$). Therefore, the ^{234}U input by α-recoil into vadose zone water is small compared to that by weathering. An exception is well S2, with $\delta^{234}U = 698‰$. In all wells, the ^{238}U activity in the dissolved fraction generally follows that of the TDS and shows no correlation with distance from the recharge area (Table 2, Fig. 4a). Note that for the wells E1(S)$_{wt}$ and E2(I), which are likely to be on a flow line (see Sect. 2), the U activity increases from 5 to 10×10^{-3} dpm/kg. However, E3(D), which we thought to be on the same flow line has a lower value than E1(S) or E2(I). Along both sampling lines, the U activity does not increase regularly and the δ^{234}U values vary between 40 and 1394‰ and do not vary regularly with distance (Fig. 4b). Although ultra-filtration experiments indicate that only 12 to 50% of the ^{238}U in filtered water pass through the 10 kD ultra-filter (Table 2), these values are lower limits (Sec. 3). Note that δ^{234}U values of the ultra-filtered fractions are always smaller than those of the corresponding filtered fraction; thus, the colloids are greatly enriched in ^{234}U and have not equilibrated with the bulk U in the water. The particulate U load was determined by measuring U in bulk and filtered waters from W3(D); the bulk water contained a slightly lower ^{238}U activity, due to some variation during pumping, and so particles generated during pumping do not contribute significantly to ^{238}U in ground water samples.

The ^{238}U activity in Magothy filtered water (18.9×10^{-3} dpm ^{238}U/kg) is in the higher range of activities from the Upper Glacial, with ≥40% of the ^{238}U in the <10 kD fraction. The ^{238}U activity in the bulk water (35.1×10^{-3} dpm/kg) shows that 46% of the total ^{238}U is associated with particles. Comparison of the δ^{234}U values in the filtered ($\delta^{234}U = 197‰$) and ultra-filtered ($\delta^{234}U = 112‰$) waters shows that, like in the Upper Glacial, colloids are enriched in ^{234}U relative to the dissolved fraction.

^{232}Th activities in Upper Glacial filtered fractions lie between 3×10^{-6} to 4×10^{-5} dpm/kg (14–165 pg/kg) (Table 2). Note that for ^{232}Th 3×10^{-6} dpm/kg = 3×10^{10} atoms/kg. There are no systematic differences between water table samples and the deeper wells. Data for sample W3(D) shows that 95% of the total ^{232}Th is carried by particles. The ^{232}Th activities are around the solubility limit (Fig. 5) of thorianite, calculated assuming there are no organic ligands and using the pH-solubility relationship of Langmuir and Herman (1980), which we consider to supercede the values given in Baes and Mesmer (1976). Note that the DOC concentrations measured in

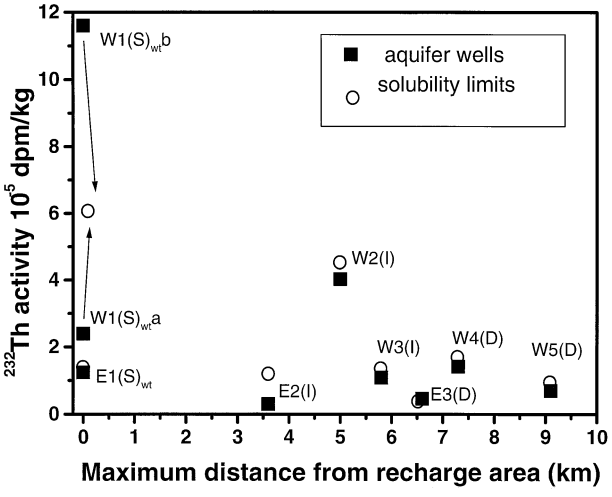

Fig. 5. ^{232}Th activities in Upper Glacial Aquifer samples versus the distance from the ground water divide (see Fig. 2). The ^{232}Th activities appear to correspond to solubility limits estimated for the corresponding pH (open circles). Solubility limits were calculated for each sampling site and were indicated for each sample. In most cases the measurement agree with the solubility limit except for sample W1(S)$_{wt}$b that is largely above the solubility limit.

Table 3. Short-lived nuclides in 0.45-μm filtered groundwater.

Well #	^{234}Th 10^{-3} dpm/kg	^{226}Ra 10^{-3} dpm/kg	^{222}Rn dpm/kg	^{228}Ra 10^{-3} dpm/kg	^{228}Th 10^{-3} dpm/kg	^{224}Ra 10^{-3} dpm/kg	^{226}Ra/^{228}Ra Activity ratio	^{224}Ra/^{228}Ra Activity ratio
West line								
W1(S)$_{wt}$	12	26 ± 6	109	37 ± 7	1.8	58 ± 12	0.7	1.6
W2(I)	15	59 ± 12	65	193 ± 38	—	145 ± 29	0.3	0.8
W3(D)	30	33 ± 6	336	42 ± 8	6.7	35 ± 7	0.7	0.8
W4(D)	26	63 ± 12	108	150 ± 30	—	159 ± 31	0.4	1.0
W5(D)	15	26 ± 6	84	45 ± 9	7.1	92 ± 18	0.6	2.1
East line								
E1(S)$_{wt}$	74	32 ± 6	174	35 ± 7	—	36 ± 7	0.9	1.0
E1$_{<10kD}$	44	<1.5	—	<5	—	<3		
E2(I)	22	22 ± 4	162	56 ± 9	—	40 ± 8	0.4	0.7
E3(D)	22	22 ± 4	522	24 ± 4	3.4	26 ± 5	0.9	1.1
Magothy								
M1	34	27 ± 6	80	45 ± 9	5.2	23 ± 4	0.6	0.5

All errors (2σ) for nuclide activities are errors equal to 20%, unless otherwise noted.

our samples might allow solubility limits that are orders of magnitude higher than the measured activities. However, there is no clear correlation between the DOC and $^{232Th}A_w$. In addition, although both nuclides are provided by weathering, the ^{232}Th/^{238}U activity ratio in the water is 10^{-2} that of the rock. This shows that ^{232}Th precipitates and that the organic matter is not a ligand controlling the Th solubility. We will not consider Th-DOC complexes in this case. The activity of one sample (W1(S)$_{wt}$) is clearly below saturation, while W1(S)$_{wt}$b collected at the same location but at a different time is above the predicted solubility limit ($\sim 2-4 \times 10^{-5}$ dpm/kg) (Table 2). This discrepancy may be due to the presence of colloids in the second sample. The Th/U ratio of the colloids in sample W3(D) is $\sim 2 \times 10^{-3}$ times that of the average continental crust, assuming all the ^{232}Th and 40% of the U (Sect. 3) are colloid-bound.

The ^{234}Th activities in the Upper Glacial $\sim 15 \times 10^{-3}$ to 74×10^{-3} dpm/kg. Due to the short half-life of ^{234}Th, ^{234}Th input from the water table does not influence the composition of deeper waters. The $^{234Th}A_w/^{238U}A_w$ ratios (^iA_w is the activity of nuclide i in the filtered water) range from 2 to 10 and show that in addition to decay of ^{238}U in the water, ^{234}Th is provided by recoil or weathering from the aquifer rock. The ratio $^{232Th}A_w/^{234Th}A_w$ in filtered waters varies by a factor of 80, reflecting the different controls on the activities of these isotopes. The data for E1(S)$_{wt}$ (Table 3) shows that 60% of ^{234}Th is in ultra-filtered water. The ^{228}Th activities in the Upper Glacial of 1.8×10^{-3} to 7.1×10^{-3} dpm/kg (Table 3) are 100 times higher than that of ^{232}Th. Therefore, ^{228}Ra decay is more important to the supply of ^{228}Th than weathering of Th from the rock. However, $^{228Th}A_w/^{228Ra}A_w \sim 0.1$ (Table 3) and so both nuclides are not in secular equilibrium.

The ^{232}Th activity in filtered water from the reduced Magothy is 21×10^{-3} dpm/kg (88 ng/kg); this is 10^3 times that of the shallow aquifer (Table 2), and therefore greatly exceeds the Th solubility limit calculated above. The DOC concentration ($\sim$5 mg/L) is comparable to that of the Upper Glacial and, as indicated previously, is not likely to account for this high activity. This water also has high Mn and Fe concentrations and ^{232}Th may then be bound to Fe-rich colloids. In contrast, the ^{234}Th (34×10^{-3} dpm/kg) and ^{228}Th (5.2×10^{-3} dpm/kg) activities are comparable to those in the Upper Glacial waters. The particulate ^{232}Th activity, deduced from bulk and filtered data, is $\sim 44 \times 10^{-3}$ dpm/kg. A similar calculation for U yields (^{232}Th/^{238}U) $\sim$2.7 for the particles, similar to upper crustal values.

These data on Th do not indicate any controlling complexation with organic matter and the activities in filtered samples generally coincide with the solubility limits of ThO_2. Therefore we consider the ^{232}Th activity in the groundwater is limited by saturation, so that once this limit is reached, ^{232}Th added by weathering is precipitated onto the surface of the aquifer solid. Changes in solubility can occur only with pH changes. In particular, due to weathering of the aquifer rock, the pH of ground waters will increase along a flow line, so that the solubility of Th will decrease, and progressive precipitation will occur. Note that our calculation of the saturation limit is based upon the assumption that ^{232}Th in the filtered water is largely dissolved. There is no data for ^{232}Th on colloids in the ground water to confirm this; however, for ^{234}Th (see below), one water table well (E1(S)$_{wt}$) appeared to have 60 ± 15% ^{234}Th in solution (Table 3) and so $\leq$ 40% of ^{232}Th is expected to be associated with colloids. At the water table, the ^{232}Th activity of one of the samples is below the calculated solubility limit. Yet, the ^{232}Th/^{238}U in the water table sample is lower than in the aquifer rocks; suggesting that if U and Th are weathered at similar rates, Th is removed more effectively than U in the vadose zone (Langmuir, 1997, Ivanovich and Harmon, 1989).

^{226}Ra activities in the Upper Glacial fall in a narrow range ($22-63 \times 10^{-3}$dpm/kg), with ^{226}Ra/^{228}Ra and ^{224}Ra/^{228}Ra ratios of 0.7 to 2.1 (Table 3). Most samples have $(22-33) \times 10^{-3}$ dpm ^{226}Ra/kg. Samples W2(I) and W4(D) are exceptions (59 and 63×10^{-3}dpm ^{226}Ra/kg), so that Ra activities alternate along the western well line (Table 3). No Ra was detected in ultra-filtered water; so Ra is carried mainly on colloids as expected for a surface-reactive element (Langmuir, 1997). However, in the "Discussion" we use the Ra activities without distinguishing between the dissolved and colloidal Ra, and the data show that adsorbed Ra is rapidly exchanging with Ra in the water. The Magothy has comparable Ra activities.

The Rn activities must be in steady state and equal to the supply rate into solution. The ^{222}Rn activities in the Upper Glacial generally vary over a narrow range of 65 to 174 dpm/kg

Table 4. Model parameters: Typical values for the upper Glacial aquifer in Long Island, New York.

Symbol	Parameter	Units
${}^iA_w$	Activity of i in the water	dpm/kg-water
${}^iA_{sc}$	Activity of i in the surface coating	dpm/kg-coating
${}^iA_r$	Activity of i in the rock (${}^{238U}A_r \sim {}^{232Th}A_r$)	440 dpm/kg-rock
${}^iA'_w$	Activity of i in the water in the vadose zone	dpm/kg-water
${}^iD$	Distribution coefficient of i between surface coating and water	
ε_i	Fraction of nuclides i produced in the rock and ejected or leached into the water after alpha-recoil	$(0.6–6) \times 10^{-5}$
f_i	Fraction of i produced in the surface coating by decay of parent p and ejected into the water	
F_i	Total fraction of i in surface coating released by desorption and ejection during production (see Appendices)	
${}^i\hat{k}_{-1}$	"Velocity" of i desorbing from surface coating	cm sec^{-1}
${}^i\hat{k}_1$	"Velocity" of i adsorbing onto surface coating	cm sec^{-1}
L_i	α-recoil length of nuclide i	2×10^{-8} m
λ_i	Decay rate of nuclide i	sec^{-1}
$S{}^i\hat{k}_1$	Removal rate of i from solution (per atom per unit volume)	
$S{}^i\hat{k}_{-1}$	Desorption rate of i from surface	
n	Porosity	0.3
q	$= n/(1 - n)$	
r	Average grain radius	$(10–100) \times 10^{-6}$ m
R_{eman}	Emanation fraction of Rn	
ρ_r	Rock density	2.7 g/cm^3
ρ_w	Water density	1 g/cm^3
ρ_{sc}	Surface coating density	2.7 g/cm^3
s	Moisture content	0–1
S	Surface coating area per volume of rock	cm^{-1}
$S\xi$	Volume of surface coating per volume of rock	
ν	Advective water velocity in the aquifer (water flux/m)	$(1–2) \times 10^{-4}$ cm · sec^{-1}
w_i	Weathering rate	sec^{-1}
ξ	Surface coating thickness	μm
χ_i	Atoms i in surface coating/atoms of i in water	
x_i	Characteristic length scale for transport of i	m

(Table 3) with higher values in W3(D) (336 dpm/kg) and E3(D) (522 dpm/kg). Such high Rn contents have been observed previously (e.g., Krishnaswami et al., 1982). The ^{222}Rn activity in the Magothy (~80 dpm/kg) is comparable to the values of the Upper Glacial. No correlation exists between ^{222}Rn and ^{238}U or ^{226}Ra. The ^{222}Rn activities are 10^3 times those of parent ^{226}Ra in the water, and cannot be produced by ^{226}Ra from the water. With a ^{226}Ra activity in the aquifer solid of 440 dpm/kg of rock and ~ 2800 dpm/kg of water (Copenhaver et al., 1993), the emanation fractions (the fraction of Rn produced by ^{226}Ra in the rock that is released into solution) are generally $(3–6) \times 10^{-2}$, with two high values of 0.12 and 0.19.

4. TRANSPORT IN THE VADOSE ZONE AND UPPER GLACIAL AQUIFER

The groundwater activities differ by several orders of magnitude, with ${}^{222Ra}A >> {}^{226Ra}A > {}^{234Th}A > {}^{234U}A \sim {}^{238U}A$, due to differences in groundwater input rates, as well as in removal rates. A transport model will be used to interpret the measured disequilibria. After a brief introduction of the model, each element will be discussed with respect to vadose zone input and aquifer transport so that the behavior of U, Th, Ra and Rn in groundwater can be characterized.

4.1. Radionuclide Transport Model

The one-dimensional model used here (Tricca et al., 2000) includes advective transport and physico-chemical reactions between three phases: water of advective velocity ν, mineral grains, and a reactive surface coating of specific surface area S and thickness ξ. All parameters used in the model are listed in Table 4 and the model is presented schematically in Figure 6. Note that each nuclide (i) in the chain is produced by its respective parent (p). This model can be applied to the average transport rate in the vadose zone by assuming that the pores are filled with water by a fraction equal to the moisture content s. The symbols used for variables in the vadose zone are the same as those in the saturated zone but with a prime. The moisture content s is unity in the saturated zone below the water table and has a value between 0 and 1 in the vadose zone.

Input of each species into the water occurs through:

- weathering characterized by a nuclide-specific weathering rate constant for the bulk rock (w_i);
- recoil ejection or preferential weathering as suggested in Hussain and Lal (1986) of a fraction ε_i of atoms produced in the rock by α-decay of parent p. Note that in case of no preferential weathering, ε_i is directly related to the radius r of the emitting mineral and to the recoil length L; for homogeneous spherical grains $\varepsilon_i \cong 3L/r$ when $L << r$ (Kigoshi, 1971). Here, $L \sim 200$ Å (Fleischer, 1982).
- production in the surface coating: f_i is the fraction of atoms i produced in the surface coating that are ejected into the water after production by α or β decay;
- desorption from the surface coating (of volume $S\xi$ per volume of rock) characterized by ${}^i\hat{k}_{-1}$ (cm sec^{-1}), the velocity of atoms i that cross the surface-water boundary to go into solution; ${}^{Th}\hat{k}_{-1}/\xi$ is equivalent to a first order kinetic constant (see Eqn. 9);

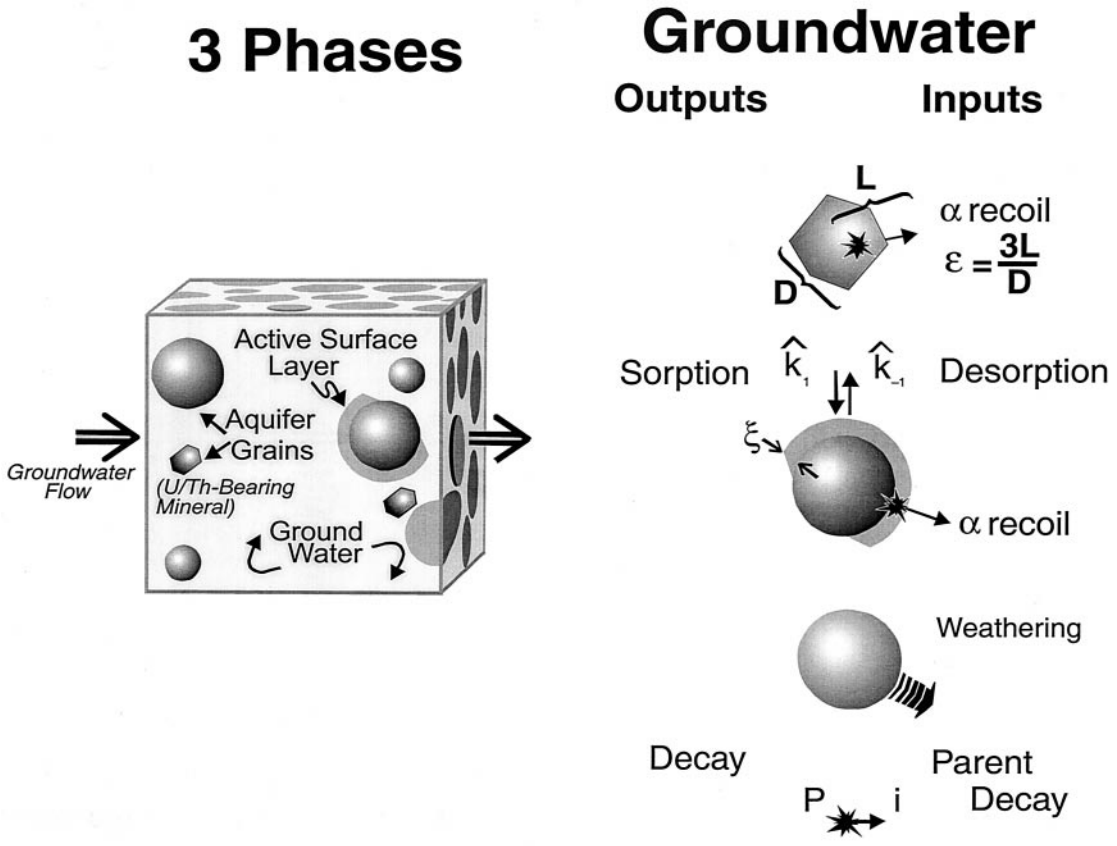

Fig. 6. Model of the aquifer and the reactions taking place between the different phases.

- decay of the parent nuclide p within the aquifer.

Removal from the water occurs through:

- decay of the nuclide within the groundwater;
- adsorption onto the surface coating characterized by ${}^{i}\hat{k}_{-1}$ (cm sec^{-1}), the average velocity with which atoms i in solution impact and sorb onto the surface layer.

We first present in Eqn. 1 (Tricca et al., 2000), the transport equation in terms of concentrations (${}^{i}c_{\beta}$) and then convert to activities (${}^{i}A_{\beta}$). This equation represents the transport in terms of mol/kg of species i in phase β (${}^{i}c_{\beta}$). The velocity of the water is the macroscopic water flux in the medium divided by the porosity and the density.

$$\frac{1}{\nu}\frac{\partial {}^{i}c_w}{\partial t}+\frac{\partial {}^{i}c_w}{\partial x}=\frac{\rho_r}{\rho_w\cdot q\cdot \nu}\cdot\left(w_i\cdot {}^{i}c_r+\varepsilon_i\cdot\lambda_p\cdot {}^{p}c_r+{}^{i}\hat{k}_{-1}\cdot\frac{\rho_{sc}\cdot S}{\rho_r}\cdot {}^{i}c_{sc}+f_i\cdot\frac{\rho_{sc}\cdot S\cdot\xi}{\rho_r}\cdot\lambda_p\cdot {}^{p}c_{sc}\right)+\frac{\lambda_p}{\nu}\cdot {}^{p}c_w-\left(\frac{\lambda_i}{\nu}+{}^{i}\hat{k}_1\cdot\frac{S}{q\cdot\nu}\right)\cdot {}^{i}c_w \quad (1)$$

As all nuclides within a decay series are linked by radioactive decay reactions, the activity of a nuclide depends on that of its precursors. To convert the concentrations to activities (${}^{i}A_{\beta}$) we multiply both sides of Eqn. 1 by λ_i and replace $\lambda_i\,{}^{i}c_{\beta}$ with (${}^{i}A_{\beta}$) and $\lambda_p\,{}^{p}c_k$ with ${}^{p}A_k$. The following transport equation for nuclide activity must be integrated for each nuclide progressively through the decay series, starting with ^{238}U and ^{232}Th.

$$\frac{1}{\nu}\frac{\partial {}^{i}A_w}{\partial t}+\frac{\partial {}^{i}A_w}{\partial w}=\frac{\rho_r}{\rho_w qs\nu}\cdot\left(w_i{}^{i}A_r+\varepsilon_i\lambda_i{}^{p}A_r+{}^{i}\hat{k}_{-1}\frac{\rho_{sc}}{\rho_r}{}^{i}A_{sc}+f_i\frac{\rho_{sc}S\xi}{\rho_r}\lambda_i{}^{p}A_{sc}\right)+\frac{\lambda_i}{\nu}{}^{p}A_w-\left(\frac{\lambda_i}{\nu}+{}^{i}\hat{k}_1\frac{S}{qv}\right){}^{i}A_w \quad (1a)$$

Here ${}^{i}A_k$ is the activity of nuclide i in phase k (water w, rock r, or surface coating sc), and ρ_k are the densities of the phases. The rock being weathered provides the source of U-Th series nuclides. We assume that the activities in the rock (${}^{i}A_r$) are constant over the time range of interest. The void ratio is $q = n/(1-n)$, where n is the porosity. At the boundary between two regions with different properties, the flux of all species (including water flow) must be conserved.

The solution to equation (1a) depends on the boundary condition at some surface and a constitutive equation describ-

ing the relationship and state of the surface coating. The variation with time of the total number of species i in the surface coating in activity units is:

$$\rho_{sc}\frac{d({}^{i}A_{sc}S\xi)}{dt} = S\rho_w {}^{i}\hat{k}_1 {}^{i}A_w + \rho_{sc}S\xi(1-f_i)\lambda_i {}^{p}A_{sc} - \rho_{sc}S({}^{i}\hat{k}_{-1}+\lambda_i\xi){}^{i}A_{sc} \quad (1b)$$

All parameters are defined in Table 4. The parameter f_i is the fraction of the production of i by decay which is lost from the surface layer by recoil. f_i is dependent on the thickness (ξ) of the surface layer with $f_i \sim 1/2$ when $\xi << L$ (the recoil distance for α decay). For production by β decay, f_i is then 1 if the daughter is not adsorbed and so completely released into solution, or 0 if it is strongly adsorbed.

There are two distinctive types of behavior of the surface layer that require attention. The simplest case is where the surface layer can exchange species with the fluid and where, for stable species, it is in local chemical equilibrium. In the steady state case, $\frac{d}{dt}({}^{i}A_{sc}S\xi) = 0$ and a relationship between ${}^{i}A_w$ and ${}^{i}A_{sc}$ is then explicitly given. This approach is similar to the usual treatment given in box model calculations. The functional form for ${}^{i}A_{sc}$ in terms of ${}^{i}A_w$ from equation (1b) can then be substituted into equation (1a) and the steady state solutions determined. A different case is when a species is saturated in the solution so that further additions above the saturation value by weathering or by production are precipitated out on the surface layer. The total number of atoms (or total activity) of this species in the surface layer ($\rho_{sc}\,{}^{i}A_{sc}S\xi$) must then increase and the surface layer is not in steady state

$$\frac{d}{dt}(\rho_{sc}\,{}^{i}A_{sc}S\xi) > 0.$$

To expand on the behavior at saturation of a species, we consider a simple box model of the aquifer with no flow and where a surface phase is growing from a solution. Then the rate constant for removal of a species from solution is $\hat{k}_1$ S/q in terms of the parameters used here. The time scale corresponding to this chemical removal is much shorter than the transit time for water motion to cover a few cm. If a system was initially saturated with a concentration of ${}^{i}c_w^{sat}$ in the water and ${}^{i}c_{sc}^{sat}$ in the surface phase, it can be shown that the addition of more species i to the water at say a constant rate $w_i\,{}^{i}c_r$ will be rapidly removed and have an excess concentration Δc_w above saturation of $\rho_r w_i\,{}^{i}c_r/\hat{k}_1 S\rho_w$. In terms of the rate constants used here, this is very small compared to ${}^{i}c_w^{sat}$. It also follows that equation (1b) becomes, for species with no precursor (e.g., ^{232}Th, ^{238}U): $\rho_{sc}\frac{d}{dt}({}^{i}A_{sc}S\xi) = \rho_r w_i\,{}^{i}A_r = \rho_w S\hat{k}_1\Delta^{i}A_w$, where $\Delta^{i}A_w \cong \lambda_i\Delta^{i}c_w$. This leads to a regular growth in the content of i in the surface coating. It also fundamentally alters the fluid transport equation. For example, if either of the parent nuclides ^{238}U and ^{232}Th are saturated, then the transport equation reduces to their saturation values ${}^{238\mathrm{U}}c_w$ or ${}^{232\mathrm{Th}}c_w$ and are not related to the weathering rate. The resulting equations for the daughter species are, in general, then different from those obtained for the exchangeable mechanism given earlier.

4.2. Transport for an Exchangeable Surface Coating

We will first develop the model of an exchangeable surface coating site and derive the general conclusions from this. It will be shown that this appears to be a reasonable description but that it is not consistent with the observation that ^{232}Th appears to be saturated. It completely fails to explain the Rn data. We will then develop a model that includes the saturation behavior of ^{232}Th and show that a model of no exchangeable sites for Th isotopes and exchangeable sites for the other nuclides appears to present a self-consistent picture.

When production from the decay of a parent within the surface coating is negligible, then at steady state we obtain from equation (1b):

$$\hat{k}_1\rho_w\,{}^{i}A_w = \rho_{sc}({}^{i}\hat{k}_{-1}+\lambda_i\xi){}^{i}A_{sc} \quad (2a)$$

The ratio of the numbers of atoms in the surface coating [$\rho_{sc}\,{}^{i}A_{sc}S\xi(1-n)$] to those in the water ($\rho_w\,{}^{i}A_w sn$) is χ_i. Using equation (2a), for a water-saturated zone ($s = 1$) we obtain:

$$\chi_i \equiv \frac{{}^{i}\hat{k}_1}{{}^{i}\hat{k}_{-1}+\lambda_i\xi}\left(\frac{S\xi}{q}\right) \equiv {}^{i}D\,\frac{S\xi}{q} \quad (2b)$$

Here ${}^{i}D \equiv {}^{i}\hat{k}/({}^{i}\hat{k}_{-1}+\lambda_i\xi)$ is the effective distribution coefficient between surface coating and the water. It may also be shown, using equation (1a) that using χ_i, there is a characteristic distance for each species $\bar{x}_i \equiv vs/\lambda_i(1+\chi_i)$.

As described in Tricca et al. (2000), the general solution to equation (1a) is of the form ${}^{i}A_w = {}^{i}A_{w0}e^{-x/\bar{x}} + {}^{i}A_{w\infty}(1-e^{-x/\bar{x}_i}) + {}^{i}J(x)$ (see Appendix A in this paper). The function ${}^{i}J(x)$, with ${}^{i}J(0) = 0$, represents the component of the activity (the 'transitional activity') of nuclide i that evolves with distance, produced by the 'transitional' decay of the precursors. The constant value of ${}^{i}A_{w\infty}$ is reached when $\lim({}^{i}J)_{x\to\infty} = 0$ and $x \gg \bar{x}_i$. The activities increase along a flow line from ${}^{i}A_{w0}$ towards a limiting value ${}^{i}A_{w\infty}$, resulting from a balance between the rate into, and the removal rate out of, the groundwater. The term ${}^{i}A_{w\infty}$ is simply the value of ${}^{i}A_w$ corresponding to the limiting case where the total rate of decay of i nuclides in the water ($\lambda_i\rho_w\,{}^{i}c_w n$) plus the surface coating ($\lambda_i\rho_{sc}S\xi(1-n)^{i}c_{sc}$) is equal to the production rate of i in the rock (both recoil and weathering) plus the production rate in the surface coating. For the case of exchangeable sites this uses equation (2b) for the ratio of the number of atoms in the surface coating to that in the water. Also note that for all reactive species that are treated here that $\chi_i >> 1$ so that $\chi_i + 1$ is extremely close to χ_i. Most of the expressions in Appendix A can be written down by inspection from the above considerations. The term ${}^{i}A_{w0}$ is the boundary condition at $x = 0$. If we take the upper boundary of the vadose zone to be at $x = 0$, then ${}^{i}A_{w0} = 0$ for all species where rainwater and dust are the input (except for ^{210}Pb, which is not treated here). For the underlying aquifer, if we take $x = 0$ to be the boundary at the water table, then ${}^{i}A_{w0}$ is the value at the base of the water table.

At steady state for ^{238}U and ^{232}Th, the primary nuclides with no parents, the solutions to equations (1a) and (1b) are of the form:

Table 5. Estimated* $\bar{x}_i$ and χ_i values for the unconfined aquifer.

Nuclide	$\bar{\tau}_i = 1/\lambda_i$ sec	χ_i	$\bar{x}_i$(m)
^{238}U	2×10^{17}	0	4.07×10^{11}
^{234}Th	3×10^{6}	700	1×10^{-2}
^{234}U	1.1×10^{13}	0	2×10^{7}
^{230}Th	3.4×10^{12}	2×10^{6}	3
^{226}Ra	7.3×10^{10}	700	3×10^{2}
^{222}Rn	4.7×10^{5}	0	9×10^{-1}
^{232}Th	6.3×10^{17}	2×10^{6}	6×10^{5}
^{228}Ra	2.6×10^{8}	100	5
^{228}Th	8.7×10^{7}	1000	9×10^{-3}
^{224}Ra	4.5×10^{5}	0.2	0.9
^{220}Rn	8.0×10^{1}	0	1.59×10^{-4}

* From model of exchangeable sites on the surface layer.

$$ {}^{i}A_w = {}^{i}A_0 e^{-x/\bar{x}_i} + \frac{\rho_r(1-n)}{n\rho_w}\frac{w_i}{\lambda_i(1+\chi_i)}\,{}^{i}A_r(1-e^{-x/\bar{x}_i}) \tag{2c} $$

As the mean lives $1/\lambda_i$ for ^{238}U and ^{232}Th are very long, it follows that even for χ_i as large as 10^6 that $x/\bar{x}_i \ll 1$ for the scale of any aquifer (see Table 5). As a result, the solution of equation (2c) reduces to the simple form:

$$ {}^{i}A_w = {}^{i}A_{w0} + \left[\frac{\rho_r(1-n)}{n\rho_w}\frac{w_i}{vs}\,{}^{i}A_r\right]x \tag{2d} $$

where we have used the definition of $\bar{x}_i$ in equation (2b). At steady state for ^{238}U and ^{232}Th, the distribution coefficient (or the retardation factor) plays no role as the surfaces are saturated.

The simplest case of a decay product is for ^{234}Th. The behavior of this short-lived nuclide can be seen from inspection of equation (1a). In the first brackets the ratio of the first term to the second term is $(w_{^{234}\mathrm{Th}}\,{}^{234\mathrm{Th}}A_r/\varepsilon_{^{234}\mathrm{Th}}\lambda_{^{234}\mathrm{Th}}\,{}^{238\mathrm{U}}A_r)$. As the rock is taken to be in secular equilibrium, the ratio of the activities is unity. For $\varepsilon_{234_{\mathrm{Th}}} \sim 5 \times 10^{-3}$ and $w_{238_{\mathrm{U}}} \sim 2 \times 10^{-16}$ sec^{-1}, the ratio of the terms is 4×10^{-6}. Thus, weathering of ^{234}Th is negligible relative to recoil. The last term within the brackets is for the decay of ^{238}U in the surface coating. As U is soluble under the conditions studied here, this term is zero. The term between the brackets represents the decay of ^{238}U in the water $(\lambda_{234_{\mathrm{Th}}}\,{}^{238\mathrm{U}}A_w/v)$. In equation (1a), the ratio of the weathering term to the ^{238}U decay in the aquifer water ($s = 1$) is $\dfrac{\rho_r}{\rho_w q}\, w_{234_{\mathrm{Th}}}\, \dfrac{{}^{234\mathrm{Th}}A_r}{{}^{238\mathrm{U}}A_w} \sim 1.5 \times 10^4$ using the data in Tables 2 and 4 and with $\varepsilon_{234_{\mathrm{Th}}} \sim 5 \times 10^{-3}$. Thus, ^{238}U decay in the water is negligible. The other terms vanish because of Eqn. 1b or 2a.

For steady state, the equation for ^{234}Th reduces to:

$$ {}^{234\mathrm{Th}}A_w \simeq {}^{234\mathrm{Th}}A_{w\infty} = \left[\frac{\rho_r}{\rho_w q}\,{}^{234\mathrm{Th}}A_r\right]\frac{\varepsilon_{^{234}\mathrm{Th}}}{(1+\chi_{^{234}\mathrm{Th}})} \tag{3} $$

Using the data on ^{234}Th in Table 3 in Eqn. 3, we find that typically $\varepsilon_{234_{\mathrm{Th}}}/\chi_{234_{\mathrm{Th}}} \sim 5 \times 10^{-6}$ in the aquifer water. For $\varepsilon_{234_{\mathrm{Th}}} = 5 \times 10^{-3}$, $\chi_{234_{\mathrm{Th}}} = 1 \times 10^3$, while for a large value of $\varepsilon_{234_{\mathrm{Th}}} = 5 \times 10^{-2}$ (Krishnaswami et al., 1982), $\chi_{234_{\mathrm{Th}}} = 1 \times 10^4$. It follows that ^{234}Th is strongly adsorbed. For a homogeneous aquifer ($^{i}A_r$ constant), then $^{234\mathrm{Th}}A_w$ should be constant. As can be seen in Table 3 the total range in $^{230\mathrm{Th}}A_w$ is constant to within a factor of two in accord with this inference.

We now estimate the ratio of the activities of ^{234}Th to ^{238}U in the water. Using Eqn. 3 for ^{234}Th and Eqn. (2d) for ^{238}U, we obtain: $^{234\mathrm{Th}}A_w/{}^{238\mathrm{U}}A_w = \nu\varepsilon_{234_{\mathrm{Th}}}/(1+\chi_{234_{\mathrm{Th}}})xw_{238_{\mathrm{U}}}$. From the values above and using $x \sim 1$ km, we find $^{234\mathrm{Th}}A_w/{}^{238\mathrm{U}}A_w \approx 5 \times 10^4/(1+\chi_{234_{\mathrm{Th}}})$. It follows that even for a high value of $\chi \sim 10^4$, the activity of ^{234}Th in the water is substantially greater than that of ^{238}U. This is what is typically observed for all aquifer samples except the Magothy (see later discussion). Only in the case where the concentration of ^{238}U in the water is exceptionally high or the removal of Th is much more efficient will $^{234\mathrm{Th}}A_w/{}^{238\mathrm{U}}A_w \sim 1$ be achieved.

[In treating ^{234}Th, we have assumed a steady state and an exchange reaction (i.e., $\hat{k}_{-1} > 0$). However, if we consider a condition where $\hat{k}_{-1} = 0$ for no transport for ^{234}Th from the surface coating to the water (i.e., irreversible precipitation), then a steady state for ^{234}Th is still possible due to the short lifetime of ^{234}Th. The value of $\chi_{234_{\mathrm{Th}}}$ would be the same as calculated above and $\chi_{^{234}\mathrm{Th}} = \dfrac{^{234\mathrm{Th}}\hat{k}_1}{\lambda_{^{234}\mathrm{Th}}} S$ corresponding to $\xi\lambda_{234_{\mathrm{Th}}} >> {}^{234\mathrm{Th}}\hat{k}_{-1}$. As we consider ^{238}U to be soluble, the above solutions for both ^{238}U and ^{234}Th are more generally applicable (see Sections 4.3 and 4.4)].

For ^{234}U, which is produced by ^{234}Th, there is a surface production term but as U is not kept in the surface layer, all terms in Eqn. (1b) vanish. The steady state problem then reduces to Eqn. (1a) for ^{234}U. All terms involving $^{238\mathrm{U}}\hat{k}_{-1}$ and $^{238\mathrm{U}}\hat{k}_1$ vanish. As $\lambda_{234_{\mathrm{U}}}$ is very small, $\dfrac{\lambda_{^{234}\mathrm{U}}}{v}\,{}^{234\mathrm{U}}A_w$ is negligible. As there is almost no ^{234}Th in the water (see above), $\dfrac{\lambda_{^{234}\mathrm{Th}}}{v}\,{}^{234\mathrm{Th}}A_w$ is negligible. The key term is $f_{^{234}\mathrm{U}}\dfrac{\rho_{sc}}{\rho_r}\mathrm{S}\xi\lambda_{^{234}\mathrm{Th}}\,{}^{234\mathrm{Th}}c_{sc}$. For this β decay, $f_{234_{\mathrm{U}}} = 1$ and using Eqn. 3, (2a), and (2b), this term becomes $\lambda_{234_{\mathrm{U}}}\varepsilon_{234_{\mathrm{Th}}}\,{}^{234\mathrm{Th}}A_r$ yielding $\dfrac{\partial}{\partial x}\,{}^{234\mathrm{U}}A_w = \dfrac{\rho_r}{\rho_w sv}(w_{^{234}\mathrm{U}}\,{}^{234\mathrm{U}}A_r + \lambda_{^{234}\mathrm{U}}\,\varepsilon_{^{234}\mathrm{Th}}\,{}^{234\mathrm{Th}}A_r)$. The solution for ^{234}U is then:

$$ {}^{234\mathrm{U}}A_w = \frac{\rho_r(1-n)}{\rho_w n}\,\frac{(w_{^{234}\mathrm{U}} + \varepsilon_{^{234}\mathrm{Th}}\,\lambda_{^{234}\mathrm{U}})}{sv}\,{}^{238\mathrm{U}}A_r \cdot x + {}^{238\mathrm{U}}w_0 \tag{4} $$

We note that as ^{238}U and ^{234}U are considered soluble, and that ^{234}Th has a short life time, that Eqn. (2d) for ^{238}U, Eqn. 3 for ^{234}Th, and Eqn. 4 for ^{234}U may be used for these nuclides as a starting point in case of saturation-precipitation of other species further down the decay series.

The approach as outlined above is applied sequentially to each of the nuclides in the decay series in determining the steady state concentrations for the exchange model.

4.3. Uranium in the Vadose Zone

We will now use the above equations to discuss the uranium isotopes. As the rainfall contributes essentially none of the nuclides under consideration (input of ^{210}Pb is important and not considered here), the input term $^{i}A_{w_0} = 0$ in the atmospheric

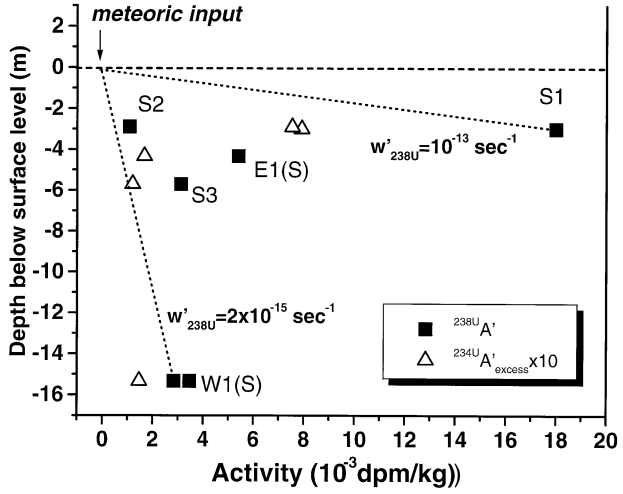

Fig. 7. ^{238}U (■) and $^{234}U_{excess}$ (Δ) activities in water table samples representing vadose zone input into the shallow aquifer. The slopes of the dashed lines give the minimum w'_{238_U} values yielding measured ^{238}U activities. Both $^{234}U_{excess}$ and ^{238}U activities in the vadose zone decrease with increasing depth. Note that the $^{234}U_{excess}$ activities at 3 m depth are identical, while the ^{238}U activities are very different.

interface with the top of the vadose zone. As discussed in Sect. 3, the vadose zone input can account for the ^{238}U in the deeper aquifer. Note that samples from water table wells are affected to a small degree by processes occurring within the aquifer; but generally contain waters that have had limited aquifer interaction. Therefore, while the input from the surrounding aquifer rock often dominates over vadose zone input for short-lived nuclides, the vadose zone contributions of the long-lived nuclides ^{238}U, ^{234}U, ^{232}Th, and ^{226}Ra remain important. In vadose zone waters (all parameters in the vadose zone will be noted with a prime), the activity $^{238}U A'_w$ is from weathering of aquifer minerals and follows the relationship:

$$^{238}\mathrm{U}A'_w = \left[\frac{\rho_r\ ^{238}\mathrm{U}A_r}{\rho_w q}\right]\left[\frac{w'_{238_U}}{sv'}\right] x \qquad (5)$$

The parameters in the second term (the moisture content s, the water velocity v', and w'_{238_U}) are highly variable, and estimated average values will be used. Within the vadose zone, where recharge by rainwater is $R \sim 50$ cm/yr, $v' = R/n'$. With $n = 0.3$ and $s = 0.5$, then the average $v' = 1 \times 10^{-5}$ cm/s. The distance x is the distance along the macroscopic flow line. The value for x that we will use (which is the distance between two sampling points on an averaged smooth flow line) therefore may well underestimate the true distance over which a stream line of water has flowed. It will be used as a first approximation in our discussion.

As seen in Figure 7, the ^{238}U activities are not linearly correlated with depth and cannot be explained by ^{238}U input by a single weathering rate constant. If a rate constant w'_{238_U} is calculated for each water table sample, then a wide range of 2×10^{-15} sec^{-1} to 1×10^{-13} sec^{-1} is obtained; these correspond to a bulk removal of (0.3-2) mg/cm^2 per yr from the vadose zone. The highest weathering rate corresponds to complete removal of the upper 3 m of the vadose zone within 2×10^5 years. The enhanced mobilization of U in the vadose zone is consistent with widely observed high chemical weathering rates in the subsurface (e.g., Langmuir, 1997), which reflect the effects of increased mechanical weathering, small grain sizes, high levels of pCO_2, and high concentrations of organic acids (see e.g., Domenico and Schwarz, 1990). These values for the sandy deposits here are somewhat lower than the average for continental chemical weathering of ~3 mg/cm^2 per yr (Garrels and McKenzie, 1971), which, however, is highly influenced by the weathering of carbonates. In general, the comparison indicates that the values obtained here for w'_{238_U} are reasonable.

Using the solution for $^{234}U A'_w$ from Eqn. 4, we obtain:

$$(^{234}\mathrm{U}A'_w/^{238}\mathrm{U}A'_w) = \frac{(w'_{234_U} + \varepsilon'_{238_{Th}}\lambda_{234_U})}{w'_{238_U}} \qquad (6)$$

Here $w'_{234_U}/w'_{238_U} \sim 1$. Using the definition of δ^{234}U, the isotopic shift (in permil deviation from secular equilibrium) in the vadose zone is:

$$\delta^{234}\mathrm{U}'_w = \left[\frac{\lambda_{234_U}\varepsilon'_{234_{Th}}}{w'_{238_U}}\right] \times 10^3 \qquad (7)$$

Note that δ^{234}U is simply related to the ratio of recoil to weathering and is independent of depth.

From the data in Table 2 samples $S1_{wt}$ and $E1(S)_{wt}$, with $\delta^{234}U \sim 30$ to 40‰ and the weathering rates calculated above, have ε' values of 6×10^{-4} to 3×10^{-2} (requiring grain sizes down to 2 μm). Well $S1_{wt}$ also has the highest ^{238}U activity, and so has the highest value for w'_{238_U}. Overall, the U data require both high weathering and high recoil rates in the shallow portion of the vadose zone. For most of the samples listed in Table 2 (see Figs. 4 and 7), there is a limited range in $\delta^{234}U'$, so that $\varepsilon'_{234_{Th}}/w'_{238_U}$ ratios are relatively constant (Eqn. 7), while the range of ^{238}U activities requires a wide range of w'_{238_U} (Eqn. 5).

The co-variation of $^{238}U A'_w$ and $\delta^{234}U'_w$ at the water table is obtained by combining Eqn. 6 and 7 to eliminate w'_{238_U}:

$$\delta^{234}\mathrm{U}'_w = \left[\frac{\rho_r\ ^{238}\mathrm{U}A_r\ \lambda_{234_U}\ \varepsilon'_{234_{Th}}10^3}{\rho_w q s v'}\right]\frac{x}{^{238}\mathrm{U}A'_w} \qquad (8)$$

This is plotted in Figure 8a for $\varepsilon'_{234_{Th}} = 5 \times 10^{-2}$ and $x = 15$ m (the maximum unsaturated zone thickness) thus establishing the possible range of vadose zone compositions. For a fixed vadose zone thickness there is thus a hyperbolic relationship between $\delta^{234}U'_w$ and $^{238}U A'_w$. For smaller x or $\varepsilon'_{234_{Th}}$, the curve shifts to downward. High values of either $^{238}U A'_w$ or $\delta^{234}U'_w$ can be obtained, but not both together. Water table data for $^{238}U A'_w$ and $\delta^{234}U'_w$ (shown in Fig. 8a) are compatible with this calculation; most samples have low $\delta^{234}U'_w$ and a range of $^{238}U A'_w$, while one sample has high $\delta^{234}U'_w$ but low $^{238}U A'_w$. Samples $S1_{wt}$ and $S2_{wt}$ fall on the calculated curve for $\varepsilon'_{234_{Th}} = 5 \times 10^{-2}$, while deeper samples in the vadose zone require $\varepsilon'_{234_{Th}} = 5 \times 10^{-3}$.

4.3.1. U transport in the unconfined aquifer

For nuclides with very long half-lives, the solution of Eqn. 1 is a curve uniformly increasing with flow distance. As noted in Sect. 3, U activities do not show such a pattern along each well

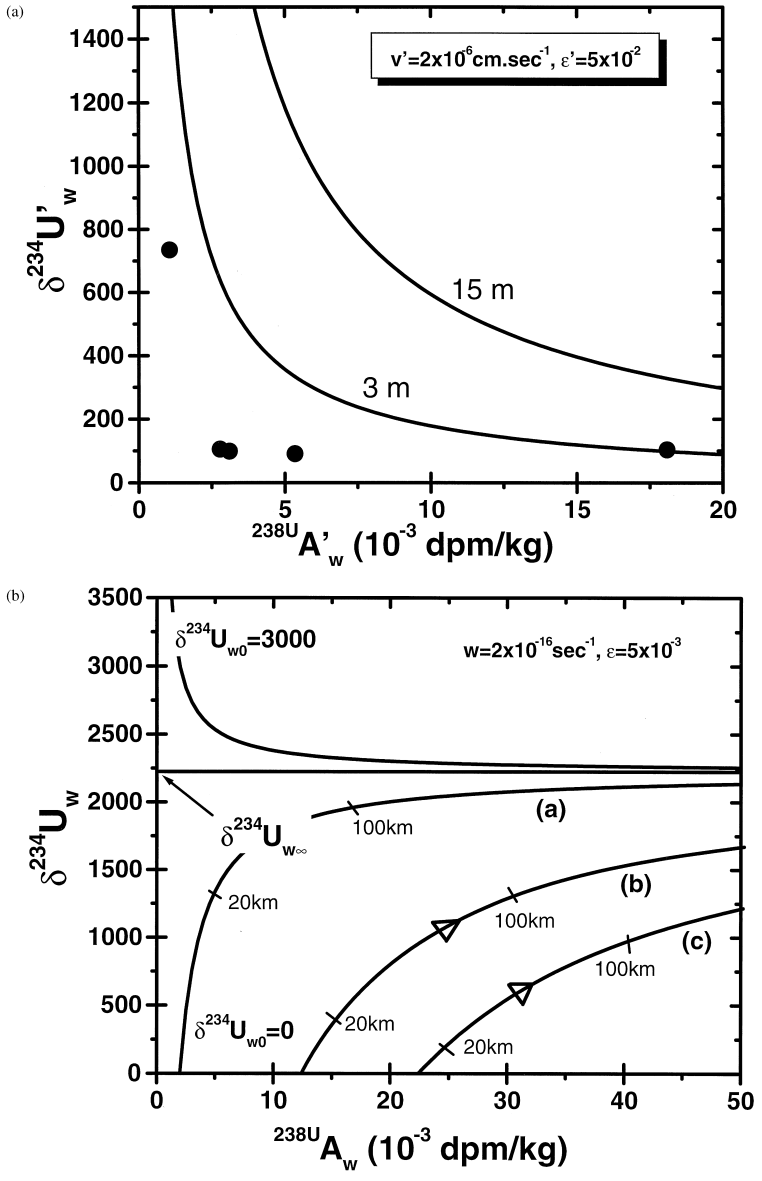

Fig. 8.a. The evolution of $\delta^{234}U'_w$ and $^{238}U A'_w$ at the water table. The curves show the model prediction for $\varepsilon'_{234_{Th}} \sim 5 \times 10^{-2}$ and for different vadose zone thicknesses (3 m and 15 m, that is the maximum thickness of the non-saturated area). Since the thickness of the vadose zone is variable, all U compositions generated in the vadose zone are located in the area below the 15m curve. The water table samples (●) are all within that region. 8b. The evolution of $\delta^{234}U_w$ and $^{238}U A_w$ along flow lines for different $\delta^{234}U_{w0}$ and $^{238}U A_{w0}$. As U is added, and the influence of the water table input diminishes, $\delta^{234}U_w$ asymptotically approaches $\delta^{234}U_{w\infty}$. In the Upper Glacial Aquifer $\delta^{234}U_{w0}$ values are likely to be $< \delta^{234}U_{w\infty}$, then $\delta^{234}U_w$ is expected to increase with U addition. Curves a, b and c are for $^{238}U A_{w0} = 2$, 12 and 22×10^{-3} dpm/kg, respectively. The flow distances are marked on each trajectory; note that these depend upon the value for w_{238_U}.

line, and so cannot be readily explained by evolution along a single flowline with uniform conditions, but rather are considered to be on different flow lines with different vadose zone inputs to the aquifer inputs. The data can be used to limit the range of conditions yielding the observed U isotope activities. The solution to Eqn. (1a) for ^{238}U, that is provided to the groundwater by input at the water table and weathering within an homogenous aquifer, is:

$$^{238}U A_w = \left(\frac{\rho_r \, ^{238}U A_r}{\rho_w q v} \right) w_{238_U} + ^{238}U A_{w0} \qquad (9)$$

Here x is the distance along a flow line, which is not actually known. The maximum x value for each sample is the distance between the well and the ground water divide to the north of the site. Figure 4a shows measured U activities versus distance from the water divide. A maximum estimate of $w_{238_U} \sim (1-7) \times 10^{-15}$ sec^{-1} is obtained from the ^{238}U activities in the aquifer, assuming no vadose zone input, $^{238}U A_{w0} = 0$. For comparison, weathering rate constants of 1 to 6×10^{-14} sec^{-1} can be obtained from the Sr data, using as the host rock Sr concentration that of the average upper crust of 350 mg/kg

(Taylor and McLennan, 1985). Since the ^{238}U in the aquifer can be provided entirely by the unsaturated zone, w_{238_U} may be much smaller.

^{234}U is provided both by weathering (along with ^{238}U) and decay of ^{234}Th going into solution. Combining the solutions of Eqn. 1a for ^{234}U and ^{238}U (and assuming $w_{234_U} = w_{238_U}$) we have:

$$\delta^{234}U = \left[\frac{\frac{\rho_r}{\rho_w q}(\lambda_{234_U}\varepsilon_{234_{Th}})\frac{^{238}U A_r}{^{238}U A_{w0}}\frac{x}{v} + \delta^{234}U_0 \times 10^{-3}}{\left(\frac{\rho_r w_{238_U}}{\rho_w q}\cdot\frac{^{238}U A_r}{^{238}U A_{w0}}\right)\frac{x}{v} + 1} \right] \times 10^3 \quad (10)$$

At long distances, an asymptotic isotope composition is approached:

$$\delta^{234}U_{w\infty} = \left(\frac{\lambda_{234_U}\varepsilon_{234_{Th}}}{w_{238_U}}\right)\cdot 10^3 \quad (11)$$

Eqn. 10 represents mixing of U supplied at the water table (with $\delta^{234}U_{w0}$ from the vadose zone) with a progressively added, aquifer-derived component with composition $\delta^{234}U_{w\infty} \propto \varepsilon_{234_{Th}}/w_{238_U}$. As both ε and w are proportional to the surface areas of the grains, changes in $\varepsilon_{234_{Th}}/w_{238_U}$ cannot be obtained by changing the mineral surface area, but rather must be due to changes in weathering reaction rates caused by changes in water or mineral chemistry (Sect. 4.2). A relationship between $\delta^{234}U$ and $^{238}U A_w$ independent of flow distance is obtained by eliminating x combining Eqn. 8 and 10 and using the vadose zone input (primes):

$$\delta^{234}U_w = (\delta^{234}U'_{w0} - \delta^{234}U_{w\infty})\frac{^{238}U A'_{w0}}{^{238}U A_w} + \delta^{234}U_{w\infty} \quad (12)$$

Samples along different distances on a flowline will fall on a trajectory defined by values for $\varepsilon_{234_{Th}}/w_{238_U}$, $\delta^{234}U_{w0}$, and $^{238}U A_{w0}$ (see Fig. 9b). If there were no vadose zone input ($^{238}U A_{w0} = 0$), $\delta^{234}U = \delta^{234}U_{w\infty}$ (a constant) and $^{238}U A_w$ would increase proportionately to distance, so that a horizontal trajectory is followed. Otherwise, $\delta^{234}U_w$ will asymptotically approach $\delta^{234}U_{w\infty}$ (Eqn. 12); whether this approach will be ascending or descending will depend upon the sign of $(\delta^{234}U_{w0} - \delta^{234}U_{w\infty})$ which depends on w_{238_U}/w'_{238_U}. As the weathering rate in the aquifer is expected to be much less than in the vadose zone, $(\delta^{234}U_{w0} - \delta^{234}U_{w\infty}) < 0$ and $\delta^{234}U_w$ increases from $\delta^{234}U'_{w0}$ upward toward $\delta^{234}U_{w\infty}$ (see Fig. 8b). Note that for the parameters used, the maximum measured value for $^{238}U A_w$ is 20×10^{-3} dpm/kg and the distance required to reach $\delta^{234}U_w$ of 2000‰ is 100 km. Consequently, only the lower part of Figure 8b is pertinent for the present discussion.

The measured ground water values of $\delta^{234}U_w$ and $^{238}U A_w$ are compared with the model in Figure 9a. Most of the Upper Glacial Aquifer well samples are in the area defined for the vadose zone input (Eqn. 5), and so the bulk of the U data in the aquifer can be explained by variability of the vadose zone with no significant input from the aquifer. However, sample W4(D) lies outside the region indicated, and so requires U input from the aquifer. No deep aquifer sample has high values for both $\delta^{234}U_w$ and $^{238}U A_w$. Note that the data do not fall on a single curve, and so cannot be explained by a single set of values for $\varepsilon_{234_{Th}}/w_{238_U}$, $\delta^{234}U_{w0}$, and $^{238}U A_{w0}$. If the vadose zone input is significantly modified by aquifer input, then U compositions of ground water can be described by Eqn. 12, and by curves shown in Figure 9a. Such trajectories are shown (curves b and c in Fig. 9a) for $\delta^{234}U_{w0} = 0$ and different $^{238}U A_{w0}$ values. The deeper aquifer data which also show high $\delta^{234}U_w$ values are close to curves for $w_{238_U} \sim 2 \times 10^{-16}$ sec^{-1}, $\varepsilon_{234_{Th}} = 5 \times 10^{-3}$, $v = 2 \times 10^{-4}$ cm sec^{-1}, $^{238}U A_{w0} = 2 \times 10^{-3}$ dpm/kg and $\delta^{234}U_{w0} = 0$. It follows that vadose zone inputs with low U concentration even with no excess ^{234}U will show substantial increase in $\delta^{234}U_w$ due to substantial recoil of ^{234}U. When $\varepsilon_{234_{Th}}/w_{238_U}$ goes up, $\delta^{234}U_w$ goes up markedly. The distance to achieve a given $\delta^{234}U_w$ depends mainly on the weathering rate. In the case of curve c where vadose zone U input is much higher, then much longer trajectories (x) are required to reach the same $\delta^{234}U_w$ (see Fig. 9b). However, the ^{238}U activity of sample W4(D) (increased by a factor of 3 with respect to the assumed initial input) and its high $\delta^{234}U_w$ value increased by more than 1000‰, requires a flow distance ~ 20 km (Eqn. 9 and 10). This is 2 times further than the distance to the ground water divide (9 km, Fig. 2). For a flow velocity that is 2 times lower, which is within the range given in Table 4, the flow distance is correspondingly reduced to 10 km. Alternatively, a higher $\delta^{234}U_{w0}$ value would readily allow achieving the W4 values; however, similar w_{238_U} and $\varepsilon_{234_{Th}}$ values are still required. Note that while a high weathering input within the aquifer could yield high $^{238}U A_w$ values, it could not generate samples with high $\delta^{234}U_w$ values. The Magothy water sample (M1) lies slightly above the vadose zone envelope and may result from, either a high $^{238}U A_{w0}$ from the vadose zone and subsequent recoil within the aquifer with low weathering rates, or a low $^{238}U A_{w0}$ and U input from the aquifer at higher weathering rates.

4.3.2. Redistribution of uranium in the vadose zone

A noteworthy feature of the U isotope distribution in the vadose zone is that both the highest ^{238}U, and highest ^{234}U excess, activities $^{234}U A'_{excess}$ were obtained for the two shallow wells, $S1_{wt}$ and $S2_{wt}$ (Figs. 7, 8a, and Table 2). The ^{238}U and excess ^{234}U activities appear to systematically decrease with increasing vadose zone thickness. An exception to this pattern is the data for one shallow well, with a relatively low ^{238}U activity but an excess ^{234}U activity comparable to the other well of same depth. That the shallowest wells have the highest $^{234}U A'_{excess}$ values may be a general feature within the vadose zone, and would suggest that high U activities are generated at shallow depths throughout the study area, with progressive removal of U from the water during downward migration. From this point of view, samples collected at locations with different vadose zone depths then represent waters that are at different stages in this evolutionary history. The highest value for $w'_{238_U} = 1 \times 10^{-13}$ sec^{-1} calculated for the top 3m, may be applicable in the upper portion of the vadose zone throughout the site. Such enhanced mobilization of U from the upper vadose zone agrees with the largely observed depletions of Fe, Al, and other elements in the A horizon due to complexation by organic humic acids (Domenico and Schwarz, 1990). The un-

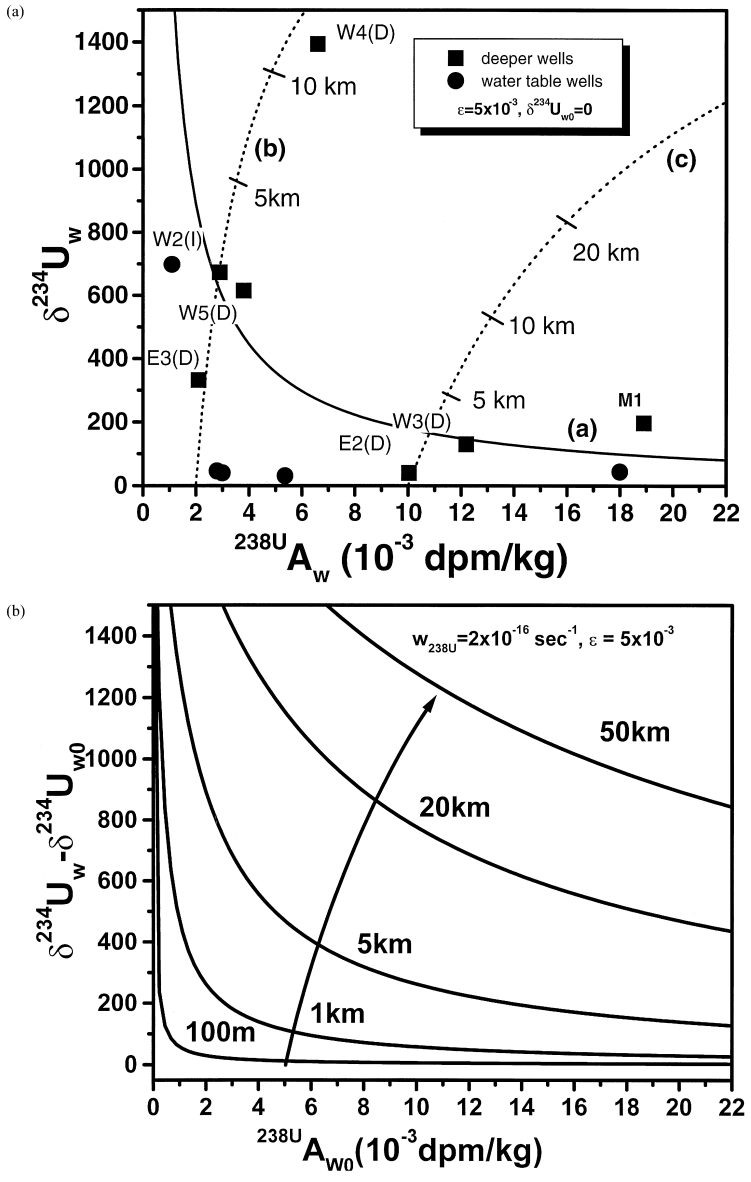

Fig. 9.a. $\delta^{234}U_w$ vs. $^{238}U A_w$ in water table (●) and deeper (■) Upper Glacial Aquifer samples. Curve a represents the envelope of the vadose zone input (calculated for the maximum thickness of the vadose zone) and shows the maximum values expected in the vadose zone; since the vadose zone thickness varies, all water table values fall below this line. Most deep well $^{238}U A_w$ values have the same range as water table values, and so may result mainly from vadose zone input. Dashed lines represent two evolutions along flow lines with flow distances marked. Curve b starts from $^{238}U A_{w0} = 2 \times 10^{-3}$ dpmU/kg a $\delta^{234}U_{w0} = 0$ and has a low w_{238_U} (2×10^{-16} sec^{-1}) and increasing $\delta^{234}U$ due to recoil input. Curve c has similar w_{238_U} and starts from $^{238}U A_{w0} = 12 \times 10^{-3}$ dpmU/kg. Note that curve b passes close to W4, which U isotopic composition obtained from this initial input requires a flow distance ~20 km. This distance can be halved if the flow velocity is twice lower than assumed here. The sample M1 from the Magothy can be explained by a high U initial activity from the vadose zone input and subsequent recoil from within the confined aquifer at low weathering rates. 9b. Distances for trajectories like curve c (Fig. 9a) but a range of values for $^{238}U A_{w0}$. Note high values for both $\delta^{234}U_w$ and $^{238}U A_w$ can only be generated over very long distances.

derlying soil layers are a sink for these less soluble constituents, forming a zone of precipitation characterized by maxima in Fe and other elements along soil profiles (Langmuir, 1997; Land, 1998; Greenman, 1999). Incorporation of U into these layers may possibly be a mechanism for U removal at depths > 3 m.

The U removal can be examined by comparing calculated U-depth profiles and the decrease in U activity below the maximum at 3 m for sample $S1_{wt}$ (Fig. 7). The model described above for radionuclide transport in ground water can be used to model removal of U including reversible adsorption onto host mineral surface coatings (see Sect. 4.1 and Figs. 6, 8a), with a $\bar{x}'_{238_U} \equiv v's/(\lambda_{238_U}(1 + \chi'_{238_U}))$(Eqn. 2b). The deep vadose zone value ~ 3×10^{-3} dpm ^{238}U/kg (Fig. 7), is reached in $\bar{x}'_{238_U} \sim$ 6 m. Then from Eqn. 2a $\chi'_{238U} > 2 \times 10^9$, which implies that 6×10^6 dpm ^{238}U/(kg of water) is associated with the surface coating in the deeper zone, and that the bulk solid has a U

concentration >1000 ppm. This is unreasonable; so, the model assumption of reversible equilibrium between the water and the surface coating is not valid. Alternatively, U removal may occur onto a surface layer that is not in steady-state equilibrium with the water. If U is removed from the water by irreversible adsorption, then ^{238}U desorption may be neglected in Eqn. 1a, so:

$$^{238}A'_w = \frac{\rho_r}{\rho_w}\frac{\bar{x}'_{238_U}}{sqv'}\,{}^{238}A_r\,(1 - q^{\frac{x}{\bar{x}'_{238_U}}}) \qquad (13)$$

where

$$\frac{1}{\bar{x}'_{238_U}} = \left(\,{}^{U}\hat{k}'_1\,\frac{S}{sqv'}\right) \qquad (14)$$

Using $\bar{x}'_{238_U} \sim 6$ m (deduced from Fig. 7), $v' \sim 5 \times 10^{-6}$ cm/s, and a void ratio $q \sim 0.5$, then $^{U}\hat{k}'_1 \sim 4 \times 10^{-9}$/S. This can be related directly to the removal rates by

$$\left[\frac{d^{238}A_w}{dt}\right]_{sorb} = -\left[\,{}^{U}\hat{k}'_1\,\frac{S}{sq}\right]{}^{238}A_w = -\left[\frac{v'}{\bar{x}'_{238_U}}\right]{}^{238}A_w \qquad (15)$$

where $(v'/\bar{x}'_{238_U})$ is the constant controlling the rate of U removal; the mean time-scale calculated for removal is then ~0.7 yrs. A corresponding weathering rate for the deep vadose zone can be obtained from Eqn. 2 of $w'_{238_U} \sim 1 \times 10^{-14}$ sec^{-1}, which is equivalent to an average weathering time of 3×10^6 years. This w'_{238_U} value is lower than the weathering rate of 1×10^{-13} sec^{-1} required to obtain the high ^{238}U activity of well $S1_{wt}$. Therefore, the vadose zone appears to be divided into an upper region (0–3 m) characterized by a high weathering rate, and the lower vadose zone (below 3m) characterized by a lower weathering rate. Note that the time-scale for removal is longer than might be expected for chemical reaction rates. A more rapid removal would imply a smaller value for $\bar{x}'_{238_U}$. If $\bar{x}'_{238_U}$ is lower by as much as a factor of 10, a uniform weathering rate would be applicable throughout the vadose zone.

The U isotopic compositions in the vadose zone vary over a limited range (Fig. 7) with the exception of one sample $S2_{wt}$, discussed further below, so that $\varepsilon'_{234_{Th}}/w'_{238_U}$ is relatively constant. Similar δ^{234}U values for the upper and lower regions of the vadose zone (where w'_{238_U} was found to decrease with depth by an order of magnitude) requires that $\varepsilon'_{234_{Th}}$ decreases with w'_{238_U}. Only an increase in the size of U-bearing grains will decrease the effective value of w'_{238_U} and keep $\varepsilon'_{234_{Th}}/w'_{238_U}$ constant. As discussed above, the higher w'_{238_U} in the upper vadose zone is likely due to differences in water chemistry, and so may have led to an overall decrease in grain size (and thus an increase in $\varepsilon'_{234_{Th}}$).

An exception to the trends discussed above is the shallow well sample $S2_{wt}$, which has a substantially lower ^{238}U activity than the other shallow well sample ($S1_{wt}$), screened at the same depth. In contrast, these wells have the same $^{234}U'_{excess}$ values (and so different $\delta^{234}U'_w$ values). This suggests that while the ^{234}U input rates by α-recoil ejection are identical at these sites, the weathering rates are different. The chemical compositions of the two samples (Table 1) also may indicate interactions with different solids.

4.4. The Behavior of Th in the Unconfined Aquifer

The first insight into the behavior of Th is seen in the measured ratios of the activities of ^{232}Th to ^{238}U. From inspection of the data in Table 2 and the discussion in Section 3, we can see that $(^{232Th}A_w/^{238U}A_w \sim (10^{-2}$ to $10^{-3})$ $(^{232Th}A_r/^{238U}A_r)$. From the exchangeable surface layer model, the ratio $(^{232Th}A_w/^{238U}A_w)/(^{232Th}A_r/^{238U}A_r) = w_{232_{Th}}/w_{238_U}$. This indicates that the weathering rate for Th is 10^{-2} to 10^{-3} that of U. This means that the intrinsic weathering rates of minerals supplying U is far greater than for those minerals supplying Th. However, this requires that U-providing minerals have extremely low Th contents. It is difficult to reconcile this with the Th/U ratios in radioactive minerals. The fact that the Th concentration of ^{232}Th appears to be fixed by the solubility limit is also in conflict with an exchange model for Th.

We follow the behavior of the isotopes for the case of an exchangeable surface coating. At steady state the solution for ^{232}Th is then given by equation (2d). Note that as $x/\bar{x}_{232_{Th}} << 1$, there is no adsorptive term. The ^{238}U decay series produces ^{230}Th. There is no ^{230}Th data yet available. However, some inferences on the ^{230}Th isotopes can be made using the data on ^{234}Th and the exchange model for ^{234}Th (see Eqn. 3) is:

$$^{234Th}A_{w\infty} = \left[\frac{\rho_r}{\rho_w q}\,{}^{234Th}A_r\right]\frac{\varepsilon_{234Th}}{(1 + \chi_{234Th})} \qquad (16)$$

If we assume $\hat{k}_{-1} >> \lambda_{234_{Th}}\xi$, (see Eqn. 2b) then $\chi_{230_{Th}} \approx \chi_{234_{Th}} = 1 \times 10^3$ to 1×10^4 and we obtain $\bar{x}_{230_{Th}} = \chi_{230}\lambda_{230}/v =$ 1.3 to 13 km. The relative importance of recoil and weathering inputs can be seen by comparing the terms in the first brackets of Eqn. 16. With $w_{230_{Th}} = w_{238_U} \leq 7 \times 10^{-15}$sec^{-1} (calculated from Table 5), $w_{230_{Th}}/\lambda_{230_{Th}} \leq 2 \times 10^{-2}$; it follows that for $\varepsilon_{230_{Th}} \sim 5 \times 10^{-3}$, either weathering or recoil could be the dominant source of ^{230}Th.

Using the asymptotic solution the maximum activity for ^{230}Th (when $x >> \bar{x}_{230_{Th}}$), we have

$$^{230Th}A_{w\infty} = \frac{\rho_r}{\rho_w q}\left(\frac{w_{230Th}/\lambda_{230Th} + \varepsilon_{230Th}}{\chi_{230_{TH}}}\right){}^{230Th}A_r \qquad (17)$$

This maximum ^{230}Th activity can be related to ^{234}Th by combining Eqn. 16 and 17:

$$\frac{^{230Th}A_{w\infty}}{^{234Th}A_{w\infty}} = 1 + \frac{w^{230}Th/\lambda_{230Th}}{\varepsilon_{230Th}} \qquad (18)$$

Therefore, an estimate of the maximum ^{230}Th activity can be obtained from the measured ^{234}Th activity from Eqn. 16. For $w_{230_{Th}} < 7 \times 10^{-15}$ sec^{-1} and $\varepsilon_{230_{Th}} = 5 \times 10^{-3}$, $^{230Th}A_{w\infty}/^{234Th}A_{w\infty} \leq 6$. If we consider a weathering rate of 2×10^{-16}sec^{-1} (corresponding to the U data) then $^{230Th}A_{w\infty}/^{234Th}A_{w\infty} \approx 1$.

A value for the desorption rate of Th from the surface coating can be obtained knowing the distribution of ^{228}Th produced by ^{228}Ac ($\tau_{1/2} = 6.2$ h) from ^{228}Ra. As there is no recoil input of ^{228}Th (produced by β decay), the dominant source for ^{228}Th is decay of ^{228}Ra in the water and desorption of ^{228}Th from the surface coating. Therefore, once the limiting activities are reached (when $x >> \bar{x}_{228_{Ra}} \approx 5$ m and $x >> \bar{x}_{228_{Ra}} \approx 1$ cm), the total activity of ^{228}Th in the water and

surface coating equals that of ^{228}Ra in these two phases. The activity of ^{228}Th in solution (correlated with the recoil supply of ^{228}Ra) is compared to that of ^{234}Th (supplied by recoil) by combining the equations for the water activities of each (see Appendix A):

$$\frac{^{228\text{Th}}A_{w\infty}}{^{234\text{Th}}A_{w\infty}} = \left[\frac{^{\text{Th}}\hat{k}_{-1} + \lambda_{^{228}\text{Th}}\xi}{^{\text{Th}}\hat{k}_{-1} + \lambda_{^{234}\text{Th}}\xi}\right] F_{^{228}\text{Th}}\left[1 + \frac{F_{^{228}\text{Ra}}\,^{232\text{Th}}N_{sc}}{\varepsilon_{^{234}\text{Th}}\,^{238\text{U}}N_r}\right] \quad (19)$$

$^{232\text{Th}}N_{sc}$ and $^{238\text{U}}N_r$ represent the number of atoms of ^{232}Th in the surface coating and ^{238}U in the rock respectively. The first bracket varies between 3×10^{-2} for very slow desorption rates and 1 in case of very rapid desorption. The second bracket represents the ^{228}Ra and ^{232}Th on the surface coating supplying ^{228}Th (direct production from the rock is negligible) relative to the ^{238}U atoms in minerals supplying ^{234}Th. We will assume that $^{\text{Th}}\hat{k}_{-1} >> \lambda_{228_{\text{Th}}}\xi$ in which case $F_{228_{\text{Th}}} \sim 1$ (see Appendix A). If the desorption rate is fast ($^{\text{Th}}\hat{k}_{-1} >> \lambda_{234_{\text{Th}}}\xi$), then $^{234\text{Th}}A_{w\infty} \geq {}^{228\text{Th}}A_{w\infty}$. However, measurements give $^{228\text{Th}}A_w/{}^{234\text{Th}}A_w = 0.1$ (Table 3) and indicate (for $^{232\text{Th}}N_{sc} \approx 0$) that $\xi/{}^{\text{Th}}\hat{k}_{-1} = 3 \times 10^7$ sec (Eqn. 19). Note that while ^{234}Th is supplied directly into solution by recoil (and then adsorbs), ^{228}Th is largely supplied into the surface coating, and the activity in solution is determined by desorption. Note that larger $\xi/{}^{\text{Th}}\hat{k}_{-1}$ values would be obtained if a significant amount of ^{232}Th existed on the surface coating. The significance of $\xi/{}^{\text{Th}}\hat{k}_{-1}$ is clearer by noting that (Tricca et al., 2000):

$$\left[\frac{d^{228\text{Th}}N_{sc}}{dt}\right]_{desorb} = \frac{^{228\text{Th}}N_{sc}(^{\text{Th}}\hat{k}_1 S)}{\xi S} = {}^{228\text{Th}}N_{sc}\left[\frac{^{\text{Th}}\hat{k}_{-1}}{\xi}\right] \quad (20)$$

Then $\xi/{}^{\text{Th}}\hat{k}_{-1} \sim 1$ yr is the mean lifetime of ^{228}Th in the surface coating. This calculation therefore provides the first estimate, based upon field measurements, of the desorption rate parameter of Th from aquifer host rock surfaces. Then, $\chi_{234_{\text{Th}}}$ should be $\sim$ 1/10 of χ_i due to its short lifetime where $i = {}^{228}$Th, ^{230}Th or ^{232}Th, and $\chi_{228_{\text{Th}}} = \chi_{230_{\text{Th}}} = \chi_{232_{\text{Th}}} = {}^{\text{Th}}\hat{k}_1/{}^{\text{Th}}\hat{k}_{-1}$ (from Eqn. 2b). The sorption rate of Th can be obtained from (Tricca et al., 2000):

$$\chi_{^{234}\text{Th}} = \frac{^{234\text{Th}}DS\xi}{q} = \frac{^{\text{Th}}\hat{k}_1 S/q}{^{\text{Th}}\hat{k}_{-1}/\xi + \lambda_{^{234}\text{Th}}} \quad (21)$$

If $\chi_{234_{\text{Th}}} = 10^3$, and assuming that $^{\text{Th}}\hat{k}_{-1}/\xi << \lambda_{234_{\text{Th}}}$ (desorption of Th is slower than decay of ^{234}Th) then $^{\text{Th}}\hat{k}_1 S/q = 3 \times 10^{-4}\text{sec}^{-1}$. Noting that adsorption follows the relationship:

$$\left[\frac{d^{228\text{Th}}N_{sc}}{dt}\right]_{sorb} = {}^{228\text{Th}}N_w\left[\frac{S^{\text{Th}}\hat{k}_1}{q}\right] = -\left[\frac{d^{228\text{Th}}N_w}{dt}\right] \quad (22)$$

a mean residence time of Th in the groundwater $\sim$ 1 h is obtained (see also Krishnaswami et al., 1982). In this treatment of exchangeable sites on the surface for Th, we see that all estimates of χ_{Th} are very large so that the surface layer always has almost all of the Th isotopes in the system surface layer plus water. As will be shown in the subsequent section, the amount of Th inferred to be on the surfaces in this model is insufficient to support the Rn.

4.5. Behavior of Ra Isotopes

The ^{226}Ra input in the vadose zone occurs by recoil and weathering of the rock; assuming exchange between the solid and the water, then for $x << \bar{x}'_{226_{\text{Ra}}}$ (see Sect. 4.1)

$$^{226\text{Ra}}A'_w = \frac{\rho_r}{\rho_w q}\,\frac{(\lambda_{^{226}\text{Ra}}\varepsilon'_{^{226}\text{Ra}} + w'_{^{226}\text{Ra}})}{v'}\,{}^{230\text{Th}}A_r \cdot x \quad (23)$$

Considering the term in the brackets, assuming $w'_{238_{\text{U}}} = w'_{226_{\text{Ra}}}$ and using $w'_{238_{\text{U}}} = 1 \times 10^{-13}$ sec^{-1} calculated for the top 3 m of the vadose zone (Sect. 4.3), then $w'_{226_{\text{Ra}}}/\lambda_{226_{\text{Ra}}} \sim 1 \times 10^{-2}$. If $\varepsilon'_{226_{\text{Ra}}} \sim \varepsilon'_{234_{\text{Th}}} \sim 2 \times 10^{-2}$, then the weathering and recoil input are comparable. At 3 m below the surface level, a ^{226}Ra activity of 32×10^{-3} dpm/kg is reached. For a thicker layer with a high weathering rate, $^{226\text{Ra}}A_w$ would increase proportionately. Consequently, the measured water table activities of ^{226}Ra ($\sim 40 \times 10^{-3}$ dpm/kg) can be reached over vadose zone thicknesses of $\geq$3 m. Since $\bar{x}'_{226_{\text{Ra}}} = 300$ m (this section and Table 5), the vadose zone input may be a dominant source of ^{226}Ra in the upper 300 m of the aquifer. The Ra isotope activities measured in two samples from the water table (Table 3) are comparable to those further down in the aquifer.

In the aquifer, the ^{226}Ra activities will be governed by the aquifer input for $x >> \bar{x}'_{226_{\text{Ra}}}$. Assuming $w_{238_{\text{U}}} \sim w_{226_{\text{Ra}}}$ then $w_{226_{\text{Ra}}}/\lambda_{226_{\text{Ra}}} << \varepsilon_{226_{\text{Ra}}}$ and recoil is the dominant input $^{226\text{Ra}}A_{w\infty} = \frac{\rho_r}{\rho_w q}\left(\frac{\varepsilon_{^{226}\text{Ra}}}{1 + \chi_{^{226}\text{Ra}}}\right){}^{230\text{Th}}A_r$ (see Appendix A). With $\varepsilon_{226_{\text{Ra}}} \sim 5 \times 10^{-3}$, $^{230\text{Th}}A_r \sim 440$ dpm/kg and no adsorption ($\chi_{226_{\text{Ra}}} = 0$), $^{226\text{Ra}}A_{w\infty} \sim 13$ dpm/kg of water. In contrast, the observed values are $\sim 30 \times 10^{-3}$ dpm/kg. Therefore the supply of ^{226}Ra by α-recoil is far more than is necessary to account for the ^{226}Ra observed in the water. Each of the Ra isotopes has quasi-constant activities in the deeper wells of the aquifer indicating that they have reached the limiting value $^{i\text{Ra}}A_{w\infty}$ (Appendix A). Here, as Ra is dominated by recoil input,

$$^{226\text{Ra}}A_{w\infty} = \frac{\rho_r}{\rho_w q}\,\frac{(\varepsilon_{^{226}\text{Ra}} + 0.5\varepsilon_{^{230}\text{Th}})}{\chi_{^{226}\text{Ra}}}\,{}^{230\text{Th}}A_r \quad (24)$$

$$^{228\text{Ra}}A_{w\infty} = \left(\frac{\rho_r}{\rho_w q}\right)\frac{\varepsilon_{^{228}\text{Ra}}\,^{232\text{Th}}A_r + 0.5\,^{232\text{Th}}A_{sc}}{\chi_{^{228}\text{Ra}}} \quad (25)$$

$$^{224\text{Ra}}A_{w\infty} = \frac{\rho_r}{\rho_w q}\,\frac{(\varepsilon_{^{224}\text{Ra}} + 0.25\varepsilon_{^{228}\text{Ra}})\,{}^{230\text{Th}}A_r + 0.25 \times 0.74\,{}^{232\text{Th}}A_{sc}}{\chi_{^{224}\text{Ra}}} \quad (26)$$

From Eqn. 24, using $\varepsilon_i \sim 5 \times 10^{-3}$ and ^{226}Ra activities between 30 to 60 $\times 10^{-3}$ dpm/kg, values of $\bar{x}_{226_{\text{Ra}}} \approx 300$ to 700 and $\bar{x}_{226_{\text{Ra}}} = 100$ to 300 m (Eqn. 2b) are obtained. Similar calculations done for ^{228}Ra and ^{224}Ra assuming that the production by ^{232}Th decay from the surface coating is negligible ($^{232\text{Th}}A_{sc} \sim 0$) lead to similar χ_{Ra} values (500–1000) as well as $\bar{x}_{228_{\text{Ra}}} \sim 7$ m and $\bar{x}_{224_{\text{Ra}}} \sim 0.3$ m (Table 5). This agrees with the well-known adsorptive behavior of Ra (e.g., Langmuir, 1997; Osmond and Ivanovich, 1992). Using the data presented in Table 3, the ^{226}Ra activity on the surface coating is calculated to be $\sim$10 dpm/kg of rock for $\chi_{\text{Ra}} = 10^3$. This surface coating activity is much less than the 440 dpm/kg ^{226}Ra inventory of the rock but is a substantial portion ($\sim$2%) of it.

Using Eqn. 24 and 25 (and if $^{232}Th A_{sc} \approx 0$), then $^{226}Ra A/^{228}Ra A \sim 1.5\ \chi_{228_{Ra}}/\chi_{226_{Ra}}$. From Eqn. 2a, $\chi_{228_{Ra}}/\chi_{226_{Ra}} \geq 1$ (also $\chi_{224_{Ra}}/\chi_{226_{Ra}} \geq 1$) so that with no contribution from the surface $^{226}Ra A_w/^{228}Ra A_w \geq 1.5$. The measured ratios of $^{226}Ra A/^{228}Ra A$ are relatively close to this value. Note that if the Ra isotopes reacted irreversibly with the surface coating, then the activity ratios in the water would be inversely proportional to the decay constants of the nuclides and the Ra activity ratios in the water would deviate by orders of magnitude from unity. As this is not the case, the assumption of reversible exchange for Ra appears to be generally valid.

All Ra isotopes have a precursor Th isotope; therefore, the parent-daughter decay pairs provide information on the relative behavior of Ra and Th. The model predicts $^{226}Ra A/^{234}Th A \sim 1.5\ \chi_{234_{Th}}/\chi_{226_{Ra}}$ (see Appendix A); the measured ratios vary from 1 to 3, and indicate that $\chi_{234_{Th}} \sim \chi_{226_{Ra}}$. Therefore, Ra and Th have similar sorption characteristics by this model. The observed relatively small variations in $^{226}Ra A_w/^{234}Th A_w$ can only be explained by a change in $\chi_{226_{Ra}}/\chi_{234_{Th}}$. Since $\chi_i \propto {}^iDS\xi$ and ${}^iD \sim {}^i\hat{k}_1/{}^i\hat{k}_{-1}$, different values of $\chi_{226_{Ra}}/\chi_{234_{Th}}$ can only occur through a change in ${}^i\hat{k}_1$ or ${}^i\hat{k}_{-1}$.

We see that the model of exchangeable sites on the surface coating appears to describe the Ra data. However, we note that the estimates of χ_{Ra} are quite critical to the question of whether there is sufficient input from the rock by recoil and weathering.

4.6. Supply of ^{222}Rn

As noted above, the exchangeable site model appears to give a reasonable semiquantitative description of the transport through the Ra isotopes, if we ignore the fact that ^{232}Th appears to be at saturation equilibrium. The radon isotopes are particularly important as this element is (when not outgassed) completely in solution. As a result, the Rn inventory is a much stricter constraint on the problem since it does not depend on a precise estimate of χ_{Rn}. Inspection of Table 3 shows that the ratio of activities of ^{222}Rn/^{226}Ra in the waters range from 10^3 to 10^4. The ratio $^{222Rn}A_{w\infty}/^{226Rn}A_{w\infty} \approx (1 + \chi_{226_{Ra}})z$. Here z represents the ratios of the recoil and weathering rates. As ^{226}Ra and ^{222}Rn are in the same chain, z is of order unity. It can be seen that the high observed ratio can only be explained by values of χ_{Ra} which are even greater than estimated above. If we use the Rn data to calculate R_{eman}, the ratio of Rn in the water phase in a volume of aquifer to the production of Rn by the rock in that same volume, we have:

$$R_{eman} = \frac{\rho_w n\, ^{222Rn}A_w}{\rho_r(1-n)\ ^{222Rn}A_r} \approx \frac{1 \times 0.3 \times 150}{2.5 \times 0.7 \times 440} = 5 \times 10^{-2} \quad (27)$$

Thus, about 5% of the total ^{222}Rn produced by the rock must be in the water phase. This would require a very high net recoil fraction of $\varepsilon \sim 5 \times 10^{-2}$. If recoil for other nuclides were this large (e.g., ^{234}U), then there would be greater δ^{234}U effects observed here.

It has been previously recognized that high ^{222}Rn activities in the water as measured here, require emanation fractions that are too high to be explained by direct recoil from typical grain sizes. This point has been earlier emphasized for instance by Krishnaswami et al. (1982) and is again confirmed here. In the present study we have included all possible contributions by both weathering and recoil as well as a reactive, exchangeable surface layer that greatly enriches the Ra content in that layer. As shown here and noted by Tricca et al. (2000), this does not provide the amount necessary to explain the high Rn levels that have been presented in the literature. Among the proposals are: the special siting of Ra within the U mineral grains to provide ready Rn losses (Krishnaswami and Seidemann, 1988; Semkov, 1990; Semkov and Parekh, 1990; Morawska and Phillips, 1992), and the existence of nanopores within a mineral and preferential diffusion of ^{222}Rn produced by ^{226}Ra (Rama & Moore, 1984; 1990). However, laboratory experiments comparing the losses of both Ar and Rn in silicate minerals failed to find any evidence for preferential diffusion (Krishnaswami and Seidemann, 1988). The authors of that work proposed that "the relatively high loss of ^{222}Rn in the samples has to be attributed to preferential enrichment of ^{226}Ra on grain surfaces or to the existence of accessory U-Th minerals in or around grain boundaries from which substantial quantities of ^{222}Rn escape." The present report has sought to provide a consistent set of relationships for all of the U-Th decay series nuclei with consideration of all contributions, including an exchangeable surface layer. However, the ^{222}Rn behavior cannot be explained with an ε_i value that is compatible with other data but requires values over a factor of ten greater. However, such an increased ε value is not compatible with observed U data as it would require a similar w_{238_U} increase. This would imply that both high δ^{234}U values and high $^{238}U A_w$ values should be easily observable in ground water samples at short distances (Fig. 8a), as the distances calculated in Sect. 4.3 decrease by a factor of 10. Therefore, while high ε_i and w_i values are valid in the vadose zone, it is not possible to apply them to all the decay series nuclides in the aquifer. The explanation of high Rn activities appears to be specific to Rn and its immediate production and other explanations have to be considered.

5. MODEL OF SATURATION-PRECIPITATION OF THORIUM

We now take into consideration the observations that:

1. ^{232}Th appears to be controlled by its saturation limit;
2. the weathering rate of ^{232}Th is very much lower than that of U for the exchangeable surface model;
3. the Ra isotopes appear to be in exchange "equilibrium" with the surface; and
4. the Rn can not be provided for by recoil, weathering and calculated Ra concentrations in the exchangeable surface layer.

Our approach is now to consider all the Th isotopes to be controlled by precipitation for additions to the water above the saturation limit for ^{232}Th; and that the surface layer, with greatly enhanced ^{232}Th and ^{230}Th, is the source of the Ra and the Rn. This results in a "mixed model" of the surface layer, dependent on the different chemical species.

To account for the Rn would require that the surface layer contain $\sim$ 10% of the ^{230}Th in the rock. The evolution of ^{232}Th for saturation is now at steady state for the water, $^{232Th}A_w = {}^{232Th}A_{wsat}$. Thus, the ratio of $^{232Th}A_w/^{238}U A_w \neq w_{232_{Th}}/w_{238_U}$. Using the discussion in Section 4 of behavior at saturation, we

have for the surface layer: $\rho_{sc}\frac{d}{dt}({}^{232\mathrm{Th}}A_{sc}S\xi) = \rho_r w_{232\mathrm{Th}}\,{}^{232\mathrm{Th}}A_r$, so that the surface layer content increases with time and:

$$\rho_{sc}({}^{232\mathrm{Th}}A_{sc}S\xi) = \rho_r w_{232\mathrm{Th}}\,{}^{232\mathrm{Th}}A_r \cdot t \tag{28}$$

As we require that at the present time, to provide the Rn, $\rho_{sc}({}^{232\mathrm{Th}}A_{sc}S\xi) \approx 10^{-1}\rho r\,{}^{232\mathrm{Th}}A_r$, this yields:

$$w_{232\mathrm{Th}}\,t = 10^{-1} \tag{29}$$

For a time scale of $\sim 10^4$ years this gives $w_{232_{\mathrm{Th}}} \sim 3 \times 10^{-13}$ sec^{-1}, which is comparable with the weathering rates found for U in some of the vadose zone samples. To obtain a weathering rate of a factor of ten lower would require a time scale of $\sim 10^5$ years which we consider too long. While the rates are compatible with a Th source in the vadose zone, the amount of Th required to coat the aquifer grains can not be provided by the vadose zone as its volume is several orders of magnitude too small. If weathering of the aquifer were to provide this amount of Th, with weathering rates typically from 2×10^{-15} to 2×10^{-16} sec^{-1}, would require time scales of 10 to 100 million years. It follows that to provide the Th inventory requires a high initial weathering rate, comparable with that of the vadose zone, and that this weathering is pervasive throughout the rock. We therefore propose that the aquifer rock originally contained two populations of U and Th minerals, one of which (called *a*) contains 10% of the U-Th inventory of the rock and undergoes rapid weathering (w_{ia}), and the other (*b*) which undergoes much slower weathering (w_{ib}). In an initial stage, the weathering input is governed by mineral "*a*" and the highly reactive nuclides from mineral "*a*" will be deposited on the surface coating.

5.1. Thorium Transport in the First Weathering Phase

From some initial state of the system the activities of all the nuclides must be found by integrating Eqn. 1a and 1b, taking into account the Th solubility limit and the weathering behavior of the U-Th phases "*a*." When phases "*a*" have been essentially exhausted by this initial weathering regime at some time *t*, then after that the ^{232}Th on the surface phase will be governed by Eqn. 28) and ^{230}Th by Eqn. 31.

At time *t*, for the short-lived ^{234}Th using Eqn. 1b and assuming that the rate constant for ^{234}Th is the same as for ^{232}Th, we have:

$${}^{234\mathrm{Th}}A_w^a \approx \frac{\rho_r\left[\varepsilon^a_{234\mathrm{Th}}\lambda_{234\mathrm{Th}} + w^a_{234\mathrm{Th}}\right]}{\rho_w S^{\mathrm{Th}}\hat{k}_1}\;{}^{238\mathrm{U}}A_r^a \tag{30}$$

For the surface coating (from Eqn. 1c)

$$\lambda_{234\mathrm{Th}}\rho_{sc}\,{}^{234\mathrm{Th}}A^a_{sc}\xi S = \rho_r(w^a_{234\mathrm{Th}} + \varepsilon^a_{234\mathrm{Th}}\lambda_{234\mathrm{Th}})\,{}^{234\mathrm{Th}}A_r^a \tag{31}$$

It can be seen that ${}^{234\mathrm{Th}}A_w$ is now related to the rate of supply by the removal rate and the connection between ${}^{234\mathrm{Th}}A_{sc}$ and ${}^{234\mathrm{Th}}A_w$ is changed. We further note that the rate constant for ^{234}Th removal from the water is ${}^{\mathrm{Th}}\hat{k}_1 S/q \sim 3 \times 10^{-4}\ \mathrm{sec}^{-1}$ (as found for the equilibrium model). This corresponds to a mean lifetime of $\sim$1 h for Th in the water.

For ^{230}Th (using Eqn. 1a and 1b and neglecting the ^{230}Th decay) the equation for the surface layer, using Eqn. 28 and 29, is given by:

$$(\rho_{sc}\,{}^{230\mathrm{Th}}A^a_{sc}S\xi) = \rho_r(w^a_{230\mathrm{Th}} + \lambda_{230\mathrm{Th}}\varepsilon^a_{230\mathrm{Th}})\,{}^{238\mathrm{U}}A_r^a \cdot t \tag{32}$$

so that

$${}^{230\mathrm{Th}}A^a_{sc}/{}^{232\mathrm{Th}}A^a_{sc} = \frac{(w^a_{230\mathrm{Th}} + \lambda_{230\mathrm{Th}}\varepsilon^a_{230\mathrm{Th}})}{w^a_{232\mathrm{Th}}}\,\frac{{}^{238\mathrm{U}}A^a_r}{{}^{232\mathrm{Th}}A^a_r} \tag{33}$$

Under the condition of rapid weathering we expect $\lambda_{230_{\mathrm{Th}}}\varepsilon^{\mathrm{a}}_{230_{\mathrm{Th}}}/w^{\mathrm{a}}_{232_{\mathrm{Th}}}$ to be much less than one. If the weathering rates of U and Th are equal ($w^a_{230_{\mathrm{Th}}} \approx w^a_{232_{\mathrm{Th}}}$), then the ratio of ^{230}Th/^{232}Th in the surface coating is the ratio in the parent rock. As the Ra isotopes are all daughters of the Th isotopes, the hypothesized surface layer would provide Ra from both series in the proper proportions. The subsequent evolution during phase *b* will then depend on the subsequent transport and production when the more resistant phases "*b*" remain.

5.2. The Present Regime with Inherited Surface Coating

After about 300 to 1000 yr (the flushing time for this aquifer), the transport equation reduces to a steady state ($\partial/\partial t = 0$) in the new regime. The governing equation is now symbolically the same as Eqn. 1b.

$$\frac{\partial\,{}^iA^*_w}{\partial x} = \frac{\rho_r}{\rho_w q s v}\cdot\left(w^i_{ib}A_{rb} + \varepsilon_{ib}\lambda_i\,{}^pA_{rb} + {}^i\hat{k}_{-1}\frac{\rho_{sc}S}{\rho_r}\,{}^iA^*_{sc} + f_i\frac{\rho_{sc}S\xi}{\rho_r}\lambda_i\,{}^pA^*_{sc}\right) + \frac{\lambda_i}{v}\,{}^pA^*_w\left(\frac{\lambda_i}{v} + {}^i\hat{k}_1\frac{S}{qv}\right)\,{}^iA^*_w \tag{34}$$

but where ${}^iA^*_{sc}$ and ${}^iA^*_w$ represent the activities of nuclide *i* in the surface coating and in the water and ${}^iA^b_r$ the rock during the second stage of weathering. A rigorous treatment would require that the activities in a different precipitated phase (i.e., different surface coatings such as ThO_2) must be described by different terms. However, this distinction is not pursued for simplicity.

The surface coating activities in Eqn. 34 depend on the integrals of Eqn. 1a and 1b during the earlier stage of weathering given above. Since the amounts of nuclides deposited during the earlier stage are presumed to be orders of magnitude higher than the ones precipitated during the later stage of lower weathering rates, ${}^iA^*_{sc}$ for long-lived reactive species that are at saturation will be dominated by the amount of nuclide *i* deposited during the earlier stage of weathering. We will assume that all other nuclides have grown back to secular equilibrium with their respective sources.

For all species that are at saturation, and because $w_{ib} << w_{ia}$, any changes in the activities (of ^{232}Th and ^{230}Th in the surface coating) due to further additions in the more recent regime will not be significant. As a result ${}^{232\mathrm{Th}}A^*_{sc}$ and ${}^{230\mathrm{Th}}A^*_{sc}$ in the present regime are the values resulting at time *t* at the end of the first regime. For exchangeable or dissolved nuclides, their activities from the earlier phase will be replaced by interaction with the water in the later phase. However, any production by the "initial" ^{232}Th-^{230}Th content in the surface

coating will have to be taken into account. Thus, in the second regime the equations governing the radium isotopes must include the ^{230}Th and ^{232}Th incorporated earlier in the surface coating. The values in the surface coating are given by Eqn. 28, 29 and 32.

The equation for ^{228}Th is found to be:

$$^{228}\mathrm{Th}A_w^b \approx \frac{\rho_r \lambda_{228\mathrm{Th}}}{\rho_w\, {}^{\mathrm{Th}}\hat{k}_1 S}\left[\varepsilon_{228\mathrm{Th}} + \frac{f_{228\mathrm{Th}}}{10}\right] {}^{232}\mathrm{Th}A_r^b \qquad (35)$$

for the case that 1/10 of the ^{232}Th inventory is on the surface coating. Using $^{\mathrm{Th}}\hat{k}_1 S/q = 3\times10^{-4}$ and $^{232\mathrm{Th}}A_r \sim 440$ dpm/kg, we obtain $^{228\mathrm{Th}}A_w \sim 1.1\times10^{-1}\left(\varepsilon_{228\mathrm{Th}} + \frac{f_{228\mathrm{Th}}}{10}\right)$. For $\varepsilon \sim 5\times10^{-3}$ and $f_{228_{\mathrm{Th}}} \sim 10^{-1}$, $^{232\mathrm{Th}}A_w \approx 1.7\times10^{-3}$ dpm/kg, which is at the low range of the observed values. If $f_{228_{\mathrm{Th}}} \sim 0.5$ (requiring a very thin surface coating) then this would cover the high range of observed values. Overall there is good agreement and self-consistency for the Th isotopic abundances. Note that $^{232\mathrm{Th}}A_w$ is typically about 1/10 of ^{228}Ra, in accord with the idea that Th is precipitated out while Ra is in exchangeable sites.

5.3. Ra and Rn from Surface Th

We now treat the radium isotopes ^{228}Ra, ^{226}Ra, and ^{224}Ra, considering them to be in exchangeable sites that are predominantly in the surface phase and that their parents were deposited during the first stage of weathering. Using Eqn. 34 at steady state in the recent regime, we obtain:

$$^{228\mathrm{Ra}}A_w = \frac{\rho_{sc}}{\rho_w\, {}^{\mathrm{Ra}}\hat{k}_1}\left[{}^{\mathrm{Ra}}\hat{k}_{-1} + f_{228\mathrm{Ra}}\,\xi\lambda_{228\mathrm{Ra}}\right] {}^{232\mathrm{Th}}A_{sc}^* \qquad (36a)$$

$$^{226\mathrm{Ra}}A_w = \frac{\rho_{sc}}{\rho_w\, {}^{\mathrm{Ra}}\hat{k}_1}\left[{}^{\mathrm{Ra}}\hat{k}_{-1} + f_{226\mathrm{Ra}}\,\xi\lambda_{226\mathrm{Ra}}\right] {}^{230\mathrm{Th}}A_{sc}^* \qquad (36b)$$

$$^{224\mathrm{Ra}}A_w = \frac{\rho_{sc}}{\rho_w\, {}^{\mathrm{Ra}}\hat{k}_1}\left[{}^{\mathrm{Ra}}\hat{k}_{-1} + f_{224\mathrm{Ra}}\,\xi\lambda_{224\mathrm{Ra}}\right] {}^{232\mathrm{Th}}A_{sc}^* \qquad (36c)$$

We showed (Eqn. 33) that $^{230\mathrm{Th}}A_{sc}^a / {}^{232\mathrm{Th}}A_{sc}^a \approx {}^{230\mathrm{Th}}A_r^a / {}^{232\mathrm{Th}}A_r^a$. As discussed in Section 4.5, if $w_{\mathrm{U}} \approx w_{\mathrm{Th}}$, the ratios of the activities of these isotopes are again all about unity. The greatest enhancement should be for ^{224}Ra which has the shortest lifetime (by over a factor of ~ 580) so that the term $f_{224_{\mathrm{Ra}}}\xi\lambda_{224_{\mathrm{Ra}}}$ makes some contribution. This may be seen in the results in Table 3. Note that the expressions in Eqn. 36a,b,c are of the form $^{\mathrm{Ra}}A_w^* = \frac{\rho_{sc} S\xi}{\rho_w q \chi_{\mathrm{Ra}}^*}\, {}^{P}A_{sc}^*$, which is identical to the form given for an exchangeable surface coating in Section 4.5 (Eqn. 24, 25, 26): $^{\mathrm{Ra}}A_w^* / {}^{\mathrm{Ra}}A_w = \frac{\rho_{sc} S \xi^P A_{sc}^* \chi_{\mathrm{Ra}}}{\rho_r \chi_{\mathrm{Ra}}^* \varepsilon_{\mathrm{Ra}}\, {}^{P}A_r}$. Since the χ_{Ra} are calculated from the same observed $^{\mathrm{Ra}}A_w$ values in both models the left hand side is equal to one. However, for the case of Th being saturated (precipitated without exchange) we have taken $\rho_{sc} S \xi^P A_{sc}^* \approx 0.1\, {}^{P}A_r$ in order to supply the Rn. It follows that $\chi_{\mathrm{Ra}}^*/\chi_{\mathrm{Ra}} \approx \frac{10^{-1}}{\varepsilon_{\mathrm{Ra}}} \sim 20$. A similar argument can be made for Th. Hence the χ_{Ra}^* values that are obtained for the Th saturation-precipitation model yield values over an order of magnitude greater than obtained earlier (i.e., $\chi_{\mathrm{Ra}}^* \sim 10^4$). This large increase in χ_{Ra} yields a change in the characteristic distances $\bar{x}_{\mathrm{Ra}}$, decreasing them by a factor of ten.

Using Eqn. 36a,b,c, the equations for Rn are then simply:

$$^{220\mathrm{Rn}}A_w^* = \frac{\rho_r}{\rho_w q}\, w^a_{^{232}\mathrm{Th}}\, {}^{232\mathrm{Th}}A_r^a \cdot t \qquad (37a)$$

$$^{222\mathrm{Rn}}A_w^* = \frac{\rho_r}{\rho_w q}\left(w^a_{^{230}\mathrm{Th}} + \lambda_{230\mathrm{Th}}\varepsilon^a_{^{230}\mathrm{Th}}\right) {}^{238\mathrm{U}}A_r^a \cdot t \qquad (37b)$$

The ratios of these activities are around unity. As we have taken $w^a_{232_{\mathrm{Th}}} \cdot t\, {}^{232\mathrm{Th}}A_r^a \approx 10^{-1} \cdot {}^{232\mathrm{Th}}A_r$ (see Eqn. 28), this will thus satisfy the ^{222}Rn observations.

5.4. Summary of Results for the Th Saturation Model

We here summarize the results obtained in this section. It was shown that if sufficient ^{232}Th and ^{230}Th are precipitated in the surface coating in non-exchangeable sites, then it is possible to explain the Ra and Rn data. However, this requires that the deposited ^{232}Th and ^{230}Th be the result of an early weathering-deposition regime before the present. If this earlier regime was of duration $t \sim 10^4$ years, then the rate of weathering is that found for the vadose zone. This weathering would have to be pervasive through the aquifer rock and cannot be provided by the present vadose zone. In the present regime, assumed to occur $\sim$ 1000 yr after the end of the initial stage of rapid weathering, the system is then described by the current input of weathering and recoil of the rock, but with the added source of ^{232}Th and ^{230}Th in the surface layer. The behavior of all nuclides except for Th isotopes is one of exchange with the surface layer, in agreement with the Ra observations. The implications of this model are that there should be a "removable" surface layer in the aquifer rock that contains $\sim$10% of the total inventory of ^{232}Th and ^{230}Th, ^{226}Ra, ^{228}Ra, and ^{224}Ra of the bulk rock system. We infer that the weathering rate for Th is about equal to that of U. The great difference between $^{238\mathrm{U}}A_w$ and $^{232\mathrm{Th}}A_w$ is due to saturation-precipitation of Th. It is also found that the characteristic distances of $\bar{x}_i$ for Ra and Th are much smaller than for the equilibrium exchange model and reduce the equations for these nuclides to a local model, approximating a "box model."

5.5. The Magothy Aquifer

As mentioned in Sect. 4, the waters within the more reducing Magothy are distinctive from those of the Upper Glacial in having Fe, Mn and Th concentrations that are orders of magnitude higher, but with Sr and U concentrations and isotopic compositions that are similar (Tables 1 and 2). These results, as well as those of the low O_2 concentrations (down by a factor of 5), show the Magothy aquifer to be more reducing and to contain a high amount of colloids. The enormous increases in Fe, Mn and Th concentrations is not directly attributable to the decrease in O_2 but is most likely due to the activity of microorganisms causing the reduction with a large effect on Fe, Mn and Th (Arnold et al., 1988). The water from the Magothy is recharged from the same area as the water from the Upper Glacial Aquifer and the flow velocities are comparable. The U isotopic composition and U activities in the Magothy are similar to those of the unconfined aquifer. Therefore, the ^{238}U and

^{234}U activities in water from the Magothy can be explained similarly to those from the Upper Glacial Aquifer (Sect. 4.3). The δ^{234}U values are constrained by the ratio $\varepsilon_{234_{Th}}/w_{238_U}$ and the U activities are dependent on the weathering rate. For instance, using a $\varepsilon_{234_{Th}} \sim 5 \times 10^{-3}$ and $w_{238_U} \sim 10^{-14}$ sec^{-1}, measured U activities in the Magothy are obtained within a few km of flow. However, the ^{232}Th activities are extremely high and $^{238}U A_w \sim {}^{232}Th A_w$ (Table 2) which indicates that U and Th input into the Magothy waters occurs by rock weathering without any fractionation or Th removal. The Ra activities (similar to those of the Upper Glacial Aquifer samples) are also shown to reflect reversible Ra adsorption onto the surface coating. The ^{222}Rn activity is at the same very high level as in the Upper Glacial Aquifer (80 dpm/kg). So ^{222}Rn data in the Magothy also require storage of Th on the surface coating during an earlier stage of weathering. The U-Th series in the aquifer economy in the Magothy is thus in consonance with the two-stage model taking into account the change in solubility of Th under somewhat reducing conditions. At present, the Th is transported on the colloids in the Magothy. This high release of Th observed in the Magothy is indicative of the fact that rather modest changes in the chemistry of an aquifer can lead to extension and rapid release of Th from what were insoluble precipitates in another circumstance. The Magothy certainly requires extensive study to understand the chemical processes involved.

6. CONCLUSIONS

The study represents a comprehensive evaluation of U- and Th-series radionuclide transport in an unconfined aquifer, and provides a model for interpreting an extensive nuclide data set measured within an aquifer. The theoretical model considerations used here are based upon a one-dimensional advective transport model considering weathering, recoil and interaction with a surface layer (Tricca et al., 2000). Values for input rates were calculated for weathering, α-recoil into the waters (both in the vadose zone and in the aquifer) and removal by adsorption/precipitation. Rate constants for adsorption and desorption were determined from the field data. Samples from water table wells have been used to evaluate input to the aquifer from the vadose zone. The activities (per kg of water) of the long-lived nuclides (^{238}U, ^{234}U, and ^{232}Th) in water table samples are comparable to those from deeper in the aquifer, demonstrating that vadose zone weathering is a dominant supply of these nuclides to the aquifer. There is a relatively wide range in measured U activities and δ^{234}U values within different water table samples. However, the vadose zone does not yield water samples with both high U activities *and* high isotopic shifts. The range in measured U activities from water table wells suggests that the upper 3 m of the vadose zone is characterized by high fractional weathering rate (w_{238_U} up to 10^{-13} sec^{-1}) and recoil radionuclide inputs (ε_i up to 5×10^{-2}) to the water. Lower weathering and scavenging of U from the water occur at locations where the vadose zone is thicker. In the aquifer, the U activities follow two trends: a wide range of U activities with low δ^{234}U values, and low U activities with higher δ^{234}U values. The variable U activities in the aquifer are thus a reflection of diverse vadose zone inputs that are preserved within the aquifer along different flow lines, rather than the result of complex non-conservative U behavior within the aquifer. Some higher δ^{234}U values for waters with low U activities in the deep aquifer show that further contribution by recoil occurs within the aquifer associated with low rates of aquifer weathering. For limited flow distances, generating high δ^{234}U requires low U input activities from the aquifer. Values of $w = 2 \times 10^{-16}$ sec^{-1} and $\varepsilon_{234_{Th}} \sim 5 \times 10^{-3}$ have been calculated to explain the measured activities in the aquifer. Observations of δ^{234}U and ^{238}U indicate that both higher w_{238_U} and $\varepsilon_{234_{Th}}$ values are not found in the aquifer. Hence, high U activities along with high δ^{234}U values cannot be attained in the ground water for the transit distances of the aquifer.

The present study provides the first groundwater data set of both long-lived ^{232}Th and short-lived ^{234}Th and ^{228}Th. The ^{232}Th activities in the groundwater appear to be controlled by the solubility of thorianite. If we assume that Th in the water is in exchange equilibrium with a surface coating with a partition coefficient, it is found that Th is strongly adsorbed. Using the ^{234}Th data, the amount of Th in the surface coating relative to that in the water (χ) is calculated to be 1×10^3. The mean residence time in the water is 1 h for Th isotopes and 1 yr in the surface coating. For Ra in the vadose zone, the main input to the water is weathering. Calculated values of $\bar{x}_{226_{Ra}} \sim 300$ m, $\bar{x}_{228_{Ra}} \sim 7$ m, and $\bar{x}_{224_{Ra}} \sim 0.3$ m indicate that while the vadose zone input of ^{226}Ra is significant in the upper portions of the aquifer, the Ra activities within the deeper aquifer are the result of local processes in the neighborhood of each sampling site. Data for ^{224}Ra, ^{226}Ra and ^{228}Ra activities show that Ra adsorbs reversibly on the surface and the calculated amount of Ra on the surface coating relative to that in the water is ≈300 to 700.

The measured activities of ^{222}Rn in the water require input of a large (~5%) fraction of the Rn produced in the solid phases as also shown by previous workers (Krishnaswami et al., 1982; Fleischer, 1982). This cannot be accounted for with the previous model, even considering contributions from a strongly adsorbing surface layer in equilibrium with the water. Ra siting on the surface of the grain has been already suggested in previous work (Krishnaswami and Seidemann, 1988), where high ^{222}Rn loss "has to be attributed to preferential enrichment of ^{226}Ra on grain surfaces or to the existence of U-Th accessory minerals in or around grain boundaries." However it is impossible to reach the required amount of ^{226}Ra by precipitation of Ra within a system in steady-state. Considering that Th appears to be at saturation limit, we propose that the source of ^{222}Rn is due to precipitation of Th at saturation and not in exchangeable sites in the surface coating. We suggest that ^{232}Th and ^{230}Th were deposited on the grain surfaces during an earlier stage of high weathering rates in the formation of the aquifer. Note that the process of dissolution, and precipitation onto the grains, of Th spatially separates ^{234}U and ^{238}U from the Ra and Th isotopes in the surface coating of the solid aquifer. This surface coating corresponds to ~ 10% of the total Th content of the rock and thereby provides the source of all daughters which are readily available to the water. Then, the effective value of Th_{sc}/Th_{water} is shown to be $\sim 5 \times 10^7$ which is a factor of 10^3 greater than in the case of exchangeable sites discussed above. It is also shown that Ra is still in exchange equilibrium with the surface coating while Th is adsorbed quasi irreversibly. The Th activities in the water are then controlled by the saturation condition. The Rn is lost by recoil or diffusion from the thin surface coating. This model predicts that ^{230}Th and ^{232}Th and

their daughter products should be removable from the surface coating by appropriate leaching techniques. From the data of Krishnaswami and Seidemann (1988), it appears that the surface layer must be formed even in granitic rocks. Therefore weathering during first exposure to the hydrosphere is considered to be responsible for forming the ThO_2 surface layer. We believe this model is broadly applicable in most geological circumstances. We cannot identify the specific rapidly weathered primary U-Th phases that are hypothesized to provide the ^{230}Th and ^{232}Th surface coatings.

We have found that Th is precipitated on surface coatings for time scales of $\sim 10^4$ years in the Upper Glacial Aquifer. However, in the underlying Magothy formation, the Th is essentially released. The water chemistry of these two aquifers is almost indistinguishable except for the drop (by a factor of $\sim$5) of the O_2 content and a concurrent increase of Fe and Mn by many powers of ten. This decrease in O_2 is plausibly the result of bacterial action. It follows that under "nearly identical" conditions, species that are fixed on surface substrates can, with a minor change in chemistry (particularly O_2), release these precipitated species. This shows that the stability of retentive sites for storage is very sensitive to changes and these sites can readily become non-retentive, particularly if in situ reduction processes may take place. We have not established a causal mechanism for this.

Acknowledgments—This work was supported by DOE grant DE-FG07 to 96ER14700. Field support from, and discussions with, J. Naidu, D. Paquette, and R. Lagatolla at BNL are appreciated. We acknowledge the extensive comments and suggestions by the reviewers that have greatly motivated us to improve the presentation. J. J. Morgan contributed to substantial improvement of the "chemistry" parts of the manuscript. The comments by M. Hoffmann on the role of bacterial action are greatly appreciated. The Brookhaven National Laboratories kindly provided access and support. Div. Contr. No. 8649(1041).

Associate editor: T. Cerlings

REFERENCES

Andrews J. N. and Kay R. L. F. (1982) ^{234}U/^{238}U activity ratio of dissolved uranium in ground waters from a Jurassic limestone aquifer in England. *Earth Planet. Sci. Lett.* **57,** 139–151.

Andrews J. N., Ford D. J., Hussain N., Trivedi D., and Youngman M. J. (1989) Natural radioelement solution by circulating groundwaters in the Stripa granite. *Geochim. Cosmochim. Acta* **53,** 1791–1802.

Arnold R. G., DiChristina T. J., and Hoffmann M. R. (1988) Reductive dissolution of Fe(III) oxides by *Pseudomonas* sp. 20. *Biotech. Bioeng.* **32,** 1081–1096.

Baskaran M., Murphy D. J., Santschi P. H., Orr, J. C., and Schink D. R. (1993) A method for rapid in-situ extraction and laboratory determination of Th, Pb and Ra isotopes from large volumes of seawater. *Deep Sea Res.* **40,** 849–865.

Chen J. H., Edwards R. L., and Wasserburg G. J. (1986) ^{238}U, ^{234}U and ^{232}Th in seawater. *Earth Planet. Sci. Lett.* **80,** 241–251.

Copenhaver S. A., Krishnaswami S., Turekian K., Epler N., and Cochran J. K. (1993) Retardation of ^{238}U and ^{232}Th decay chain radionuclides in Long Island and Connecticut aquifers. *Geochim. Cosmochim. Acta* **57,** 597–603.

Cowart J. B. and Burnett W. C. (1994) The Distribution of Uranium and Thorium Decay-Series Radionuclides in the Environment—a Review. *J. Env. Qual.* **23(4),** 651–662.

Davidson M. R. and Dickson B. L. (1986) A porous flow model for steady state transport of radium in groundwater. *Wat. Resour. Res.* **22,** 34–44.

de Laguna W. (1963) Geology of Brookhaven National Laboratory and Vicinity, Suffolk County, New York. *U.S.G.S. Bull.* **1156-A,** 35 p.

de Laguna W. (1966) A hydrologic analysis of postulated liquid-waste releases, Brookhaven National Laboratory and Vicinity, Suffolk County, New York. *U.S.G.S. Bull. 1156D,* 51 p.

Domenico P. A. and Schwartz F. W. (1990) Physical and Chemical Hydrogeology. Wiley.

Faust G. T. (1963) Physical Properties and Mineralogy of Selected Samples of Sediments from the Vicinity of the Brookhaven National Laboratory, Long Island, N.Y. *U.S.G.S. Bull. 1156B.*

Fleischer R. L. (1982) Alpha-recoil damage and solution effects in minerals: uranium isotopic disequilibrium and radon release. *Geochim. Cosmochim. Acta* **46,** 2191–2201.

Fox L. E. (1988) The solubility of colloidal ferric hydroxide and its relevance to iron concentrations in river water. *Geochim. Cosmochim. Acta* **52,** 771–777.

Garrels R. M. and Mackenzie F. T. (1971) Evolution of sedimentary rocks. New York, Norton.

Gascoyne M. (1992) Geochemistry of the actinides and their daughters. In *Uranium-series Disequilibrium* (ed. Ivanovich and Harmon), pp. 34–61. Oxford Science Publications.

Geraghty and Miller. (1996) Regional Groundwater Model, Brookhaven National Laboratory, Upton, New York. Geraghty and Miller Inc., Melville, NY.

Hem J. D. (1992) Study and Interpretation of the Chemical Characteristics of Natural Water. *U.S.G.S. Water-Supply Paper 2254.*

Hubbard N., Laul J. C., and Perkins R. W. (1984) The use of natural radionuclides to predict the behavior of waste radionuclides in far-field aquifers. Proceedings of scientific basis for nuclear waste management V, Amsterdam (ed. W. Lutze).

Hussain N. and Lal D. (1986) Preferential solution of ^{234}U from recoil tracks and ^{234}U/^{238}U radioactive disequilibrium in natural waters. *Proc. Indian Acad. Sci. (Earth Planet. Sci).* **95,** 245–263.

Kigoshi K. (1971) Alpha-recoil thorium-234: dissolution into water and the uranium-234/uranium-238 disequilibrium in nature. *Science* **173,** 47–48.

Krishnaswami S., Graustein W. C., Turekian K. K., and Dowd J. F. (1982) Radium, thorium and radioactive lead isotopes in groundwaters: Application to the in situ determination of adsorption-desorption rate constants and retardation factors. *Water Res. Res.* **18,** 1663–1675.

Krishnaswami S. and Seidemann D. E. (1988) Comparative study of ^{222}Rn, ^{40}Ar, ^{39}Ar and ^{37}Ar leakage from rocks and minerals. Implication for the role of nanopores in gas transport through natural silicates. *Geochim. Cosmochim. Acta* **52,** 655–658.

Ku T. L., Luo S., Leslie B. W., and Hammond D. E. (1992) Decay-series disequilibria applied to the study of rock-water interaction and geothermal systems. In *Uranium-series Disequilibrium* (ed. M. Ivanovich and R. S. Harmon). Oxford Science Publication.

Land M. (1998) Weathering of till in northern Sweden and its implications for the geochemistry of soil water, groundwater, and stream water. Ph.D. thesis, Luleå Inst. Tech., Luleå, Sweden.

Langmuir D. (1997) Aqueous environmental geochemistry. Prentice Hall, NY.

Langmuir D. and Herman J. S. (1980) The mobility of thorium in natural waters at low temperatures. *Geochim. Cosmochim. Acta* 44, 1753–1766.

National Atmospheric Deposition Program, (1998) *National Atmospheric Deposition Program, 1997 Wet Deposition.* Illinois State Water Survey, Champaign, IL.

Osmond J. K. and Cowart J. B. (1992) Groundwater. In *Uranium-series Disequilibrium* (ed. M. Ivanovich and R. S. Harmon). Oxford Science Publ.

Osmond J. K. and Ivanovich M. (1992) Uranium-series mobilization and surface hydrology. In *Uranium-series Disequilibrium* (ed. M. Ivanovich and R. S. Harmon). Oxford Science Publ.

Porcelli D., Andersson P. S., Wasserburg G. J., Ingri J., and Baskaran M. (1997) The importance of colloids and mires for the transport of uranium isotopes through the Kalix River watershed and Baltic Sea. *Geochim. Cosmochim. Acta.* **61,** 4095–4113.

Rama and Moore W. S. (1984) Mechanism of transport of U-Th series of radioisotopes from solids into groundwater. *Geochim. Cosmochim. Acta* **48,** 395–399.

Rama and Moore W. S. (1990) Submicronic porosity in common minerals and emanation of radon. *Nuc. Geophys.* **4,** 467–473.

Reid D. F., Key R. M., and Schink D. R. (1979) Radium, thorium and

actinium extraction from sea-water using an improved manganese-oxide-coated fiber. *Earth Planet. Sci. Lett.* **43,** 223–226.
Semkov T. M. (1990) Recoil-emanation theory applied to radon release from mineral grains. *Geochim. Cosmochim. Acta* **54,** 425–440.
Semkov T. M. and Parekh P. P. (1990) The role of radium distribution and porosity in radon emanation from solids. *Geophys. Res. Lett.* **17,** 837–840.
Stumm W. and Morgan J. J. (1996) Aquatic Chemistry. Wiley Interscience.
Taylor S. R. and McLennan S. M. (1985) The Continental Crust: Its Composition and Evolution. Blackwell, Oxford.
Tricca A., Porcelli D., and Wasserburg G. J. (2000) Factors controlling the ground water transport of U, Th, Ra and Rn. In *Gopalan Festschrift Volume* (ed. Y. J. B. Rao et al.), vol 109. Proceedings of the Indian Academy of Science.
Warren M. A., de Laguna W., and Lusczynski N. J. (1968) Hydrology of Brookhaven National Laboratory and Vicinity, Suffolk County, New York. *U.S.G.S. Bull. 1156C,* 127 p.

APPENDIX A

^{238}U-SERIES:

- $$^{238}A_{w\infty} = \left(\frac{\rho_r}{\rho_w \cdot q}\right) \frac{w_{^{238}U}}{\lambda_{^{238}U}} \; ^{238}A_r$$
- $$^{234}A_{w\infty} = \left(\frac{\rho_r}{\rho_w q}\right) \frac{(w_{^{234}Th} + \varepsilon_{^{234}Th}\lambda_{^{234}Th})}{\lambda_{^{234}Th}(1 + \chi_{^{234}Th})} \; ^{238}A_r$$
- $$^{234}A_{w\infty} = \left(\frac{\rho_r}{\rho_w q}\right) \frac{\left(w_{^{234}Th} + w_{^{234}Th}\frac{\lambda_{^{234}U}}{\lambda_{^{234}Th}} + \varepsilon_{^{234}Th}\lambda_{^{234}U}\right)}{\lambda_{^{234}U}} \; ^{238}A_r$$
- $$^{230}A_{w\infty} = \frac{\rho_r}{\rho_w q} \frac{(w_{^{230}Th} + \varepsilon_{^{230}Th}\lambda_{^{230}Th})}{\lambda_{^{230}Th}(1 + \chi_{^{230}Th})} \; ^{238}A_r$$
- $$^{226}A_{w\infty} = \frac{1}{1 + \chi_{^{226}Ra}}\left(\frac{\rho_r}{\rho_w q}\left(\frac{w_{^{226}Ra}}{\lambda_{^{226}Ra}} + \varepsilon_{^{226}Ra}\right) {}^{230}A_r + F_{^{226}Ra}\chi_{^{230}Th} \; ^{230}A_{w\infty}\right)$$
- $$^{230}A_{w\infty} = \frac{\rho_r}{\rho_w q}\left(\varepsilon_{^{222}Rn} + f_{^{222}Rn}\left(\frac{w_{^{226}Rn}}{\lambda_{^{226}Rn}} + \varepsilon_{^{226}Ra} + (1 - f_{^{226}Ra})\left(\frac{w_{^{230}Th}}{\lambda_{^{230}Th}} + \varepsilon_{^{230}Th}\right)\right)\right) {}^{238}A_r$$

^{230}Th-SERIES:

- $$^{232}A_{w\infty} = \frac{\rho_r}{\rho_w q}\left(\frac{w_{^{232}Th}}{\lambda_{^{232}Th}(1 + \chi_{^{232}Th})}\right) {}^{232}A_r$$
- $$^{228}A_{w\infty} = \frac{\rho_r}{\rho_w q} \frac{\left(\frac{w_{^{228}Ra}}{\lambda_{^{228}Ra}} + \varepsilon_{^{228}Ra} + F_{^{228}Ra}\frac{w_{^{232}Th}}{\lambda_{^{232}Th}}\right)}{1 + \chi_{^{228}Ra}} \; ^{232}A_r$$
- $$^{224}A_{w\infty} = \frac{\rho_r}{\rho_w q} \frac{\left(\frac{w_{^{228}Th}}{\lambda_{^{228}Th}} + F_{^{228}Ra}\left(\frac{w_{^{228}Ra}}{\lambda_{^{228}Ra}} + \varepsilon_{^{228}Ra} + (1 - f_{^{228}Ra})\frac{w_{^{232}Th}}{\lambda_{^{232}Th}}\right)\right)}{(1 + \chi_{^{228}Th})} \; ^{232}A_r$$

$$^{224}A_{w\infty} = \frac{\rho_r}{\rho_w q} \frac{\left(\frac{w_{^{224}Ra}}{\lambda_{^{224}Ra}} + \varepsilon_{^{224}Ra}\right)}{1 + \chi_{^{224}Ra}} \; ^{228}A_r$$

$$+ \frac{F_{^{224}Ra}\chi_{^{228}Th}}{1 + \chi_{^{224}Ra}} \; ^{228}A_{w\infty} + \frac{F_{^{224}Ra}(1 - f_{^{228}Th})\left(\frac{\lambda_{^{228}Th}\xi}{{}^{Th}\hat{k}_{-1} + \lambda_{^{228}Th}\xi}\right)\chi_{^{228}Ra}}{1 + \chi_{^{224}Ra}} \; ^{228}A_{w\infty}$$

$$+ \frac{F_{^{224}Ra}(1 - f_{^{228}Th})\left(\frac{\lambda_{^{228}Th}\xi}{{}^{Th}\hat{k}_{-1} + \lambda_{^{228}Th}\xi}\right)(1 - f_{^{228}Ra})\left(\frac{\lambda_{^{228}Ra}\xi}{{}^{Ra}\hat{k}_{-1} + \lambda_{^{228}Ra}\xi}\right)\chi_{^{232}Th}}{1 + \chi_{^{224}Ra}} \; ^{232}A_{w\infty}$$

and $F_i \equiv \left((1 - f_i)\left(\frac{{}^{Th}\hat{k}_{-1}}{{}^{Th}\hat{k}_{-1} + \lambda_i\xi}\right) + f_i\right)$